Near-field dynamics of parallel twin jets in cross-flow

Cite as: Phys. Fluids **29**, 035103 (2017); https://doi.org/10.1063/1.4978856
Submitted: 25 October 2016 . Accepted: 07 March 2017 . Published Online: 23 March 2017

B. Zang, and T. H. New

Near-field dynamics of parallel twin jets in cross-flow

B. Zang and T. H. New[a)]
School of Mechanical and Aerospace Engineering, Nanyang Technological University, 50 Nanyang Avenue, Singapore 639798, Singapore

(Received 25 October 2016; accepted 7 March 2017; published online 23 March 2017)

The present study examines the near-field flow developments and dynamics of parallel twin jets in cross-flow (TJICF) configured with jet-to-jet separation distances of 1.5 to 3 jet diameters (D) and velocity ratios of 2, 4, and 6. Both laser-induced fluorescence and particle-image velocimetry measurements were made along the streamwise and cross-stream planes in order to investigate the effects of the separation distance and velocity ratio upon the deflected jet and the formation of counter-rotating vortex-pairs (CVPs) within the near-field region. Results show that each jet in the parallel TJICF configuration attains higher cross-flow entrainment and produces greater jet half-widths than a single jet in cross-flow (SJICF). Moreover, as the separation distance decreases to 1.5D, the twin jets interact closer to the jet exit such that organized leading-edge and lee-side vortices are present along the symmetry plane. Cross-stream results indicate that the pair of inner vortices associated with the two resulting CVPs is being induced to move towards each other along the symmetry plane, where their opposite-signed vorticities annihilate with each other eventually. As such, the vorticity transition from two CVPs into a resulting single CVP takes place quickly within the near-field region when the separation distance is sufficiently small. Streamwise circulation decays determined for parallel TJICF show that their circulations increase moderately when the two CVPs begin to interact with each other. Further examination into the Reynolds shear stresses indicates that there exists substantial flow shear stress as the pair of inner vortices interacts, which yields higher entrainment level of the cross-flow fluid in regions adjacent to the symmetry plane. As a result, the near-field jet trajectories for each jet in the parallel TJICF are always lower than that of the corresponding SJICF when the separation distance is small, regardless of the velocity ratios. *Published by AIP Publishing.* [http://dx.doi.org/10.1063/1.4978856]

I. INTRODUCTION

When a jet discharges transversely into a free-stream to produce a jet in cross-flow (JICF) phenomenon, it is known that continual interactions between the jet and the cross-flow produce four prominent vortical systems in the near- and far-field regions, namely, the leading-edge and lee-side vortices, the counter-rotating vortex pair (CVP), the horseshoe, and the wake vortices. These large-scale coherent structures essentially govern the flow dynamics of a JICF and have been the subjects of interest in numerous studies over the past seventy years (Margason, 1993 and Mahesh, 2013). This is not only due to the wide range of engineering applications that utilize JICF configurations but also due to significant scientific curiosity surrounding this fundamental flow phenomenon. Some typical examples of engineering applications that make use of JICF phenomenon would include film cooling of turbine blades, fuel injection system in gas burners, and vector thrust control of VTOL/ASTOVL aircrafts, take for instance.

Flow developments associated with the large-scale vortical structures of a circular single jet in cross-flow (SJICF) have been examined extensively in the literature. As the circular jet penetrates into a cross-flow, it deflects towards the cross-flow direction due to the presence of an adverse pressure gradient and constant entrainment of the cross-flow fluid. As such, it has been determined that the JICF trajectory is strongly associated with the momentum ratio between the jet and the cross-flow (Pratte and Baines, 1967 and Muppidi and Mahesh, 2005). On the other hand, leading-edge and lee-side vortices result from the hydrodynamic wave instabilities along the deflected jet shear layer (i.e., also known as Kelvin-Helmholtz instabilities), shortly after the jet exhausts from the jet exit (Kelso *et al.*, 1996 and Lim *et al.*, 2001). The CVP also initiates close to the jet exit but only develops into the dominant coherent structure in the far-field region as the jet vorticity realigns itself with the cross-flow (Fearn and Weston, 1974; Broadwell and Breidenthal, 1984; and Fric, 1990). The transition of the jet vorticity into a CVP structure takes place rather rapidly within the near-field and the CVP is known to persist at significant distances downstream of the jet exit, where its circulation decays gradually with an approximate power law relation (Nun, 1985 and Karagozian, 1986). Due to its far-field dominance and impact upon the overall jet-mixing efficacy, various flow models had been proposed by researchers to better elucidate this transition process by invoking concepts associated with vortex-rings, vortex-loops, or pressure gradient (Kelso *et al.*, 1996; Yuan *et al.*, 1999; Cortelezzi and Karagozian, 2001; Lim *et al.*, 2001; Muppidi and Mahesh, 2006; Marzouk

[a)]Author to whom correspondence should be addressed. Electronic mail: dthnew@ntu.edu.sg

and Ghoniem, 2007; and Cambonie *et al.*, 2013). Readers are encouraged to refer to the review by Margason (1993), Mahesh (2013), and Karazogian (2014) for more details on the various aspects of the circular SJICF flow phenomenon.

Since one of the primary interests in JICF phenomenon is the ability of the deflected jets to entrain and mix with the cross-flow fluid, jet exit geometries other than circular ones have been explored to manipulate and possibly improve upon such characteristics. For instance, jets issuing from square, rectangular, and elliptical geometries into cross-flows have been investigated in terms of the influences of the jet geometries upon the near-field jet dynamics and formation of CVPs. These studies included Haven and Kurosaka (1997), Ajersch *et al.* (1997), Zaman and Foss (1997), Gogineni *et al.* (1998), Findlay *et al.* (1999), Holdeman *et al.* (1999), New *et al.* (2003, 2004), Lim *et al.* (2006), and New (2008). In general, non-uniform distributions of jet exit momentum due to the use of noncircular jet exit geometries led to significant differences in the interactions between the jet and the cross-flow. In particular, the exact orientations of the jet exit with respect to the cross-flow direction, possible presence of corners, and strong self-induced velocities in some of these noncircular jet exit geometries were observed to introduce complex three-dimensional flow behaviour which could possibly be exploited further in order to realize better entrainment and mixing levels.

On the other hand, it will also be intuitive to try to achieve higher mixing levels by exhausting more than one jet into a cross-flow simultaneously, as demanded by selected engineering applications as well. By locating the multiple jets relatively close to one another, mutual interactions between adjacent jet flows become significant and potentially further complicating the underlying dynamics of the flow. This is true even for multiple free jets without the presence of a free-stream, as an earlier study by the authors demonstrates (Zang and New, 2015). Naturally, earlier investigations on multiple JICF focused on the effects of jet number and their spacing upon the mixing between the jet and ambient fluid. Holdeman and Walker (1977) investigated the temperature distributions downstream of a parallel row of cooling jets injected transversely into a heated cross-flow in a confined channel. By varying the momentum ratio, jet-to-jet spacing, and jet number, respectively, they concluded that the momentum ratio remains an important independent variable in the jet penetration and mixing with the hot cross-flow. Furthermore, decreasing the spacing between two adjacent jets would promote cooling of the hot cross-flow fluid along the streamwise mid-plane. More interestingly, their results suggested that the temperature distribution would remain relatively unaffected when the jet-to-jet separation was increased to six jet diameters (D) and beyond.

Toy *et al.* (1993) also experimentally investigated parallel twin jets in cross-flow (TJICF) at a velocity ratio of 6 and a jet-to-jet separation of 5D. From the video images and pressure field measurements at locations between 10D and 25D downstream of the jet exit, they found that only a single CVP could be observed and that it dominated the far-field region of the parallel TJICF. These observations led them to recommend further examinations into the near-field flow developments of parallel TJICF at smaller jet-to-jet separations in order to reveal greater details on the CVP interactions. Later, Schlüter and Schönfeld (2000) replicated the flow conditions used by Toy *et al.* (1993) in their large-eddy simulation investigation of parallel TJICF. Their findings led them to infer that the inner pair of vortices from the two CVPs, being spatially close to each other, experiences Coanda's effects and subsequently broke down into smaller vortices that dissipate as the parallel TJICF convect downstream.

More recent experimental studies on parallel TJICF by Kolář *et al.* (2003) and Kolář and Savory (2007) emphasized the quantitative measurements of their far-field vorticity distributions and circulation decay through hot-wire anemometry. Employing a configuration similar to that of Toy *et al.* (1993) but with a higher velocity ratio of 8, they found that there exists an approximately linear relationship between the growth of the CVP width and streamwise distance beyond 10D, which was quite reminiscent of a SJICF. Further analysis on the CVP circulation decay revealed comparable strengths between the SJICF and parallel TJICF CVPs at the far-field region. Their measurements corroborated the fact that a single CVP would eventually emerge in the far-field region of parallel TJICF, presumably as a direct result of the constant interactions between the two CVP structures.

Nevertheless, these observations from the previous studies raise further questions and scientific curiosity on the flow interactions and transitions taking place between the two CVPs in the near-field of a parallel TJICF. Moreover, it is evident from the foregoing discussions that investigations into the near-field dynamics of parallel TJICF large-scale coherent structures remain relatively limited as compared to the SJICF scenario. More detailed measurements on the near-field region of a parallel TJICF will thus provide timely insights and knowledge on their dynamics and developments. In particular, a study on parallel TJICF with jet-to-jet separation distances comparatively smaller than those used in earlier studies will provide further useful information towards our overall understanding of multiple JICF flow behavior, as pointed out by Toy *et al.* (1993). To address these motivations, an experimental study on parallel TJICF has been carried out to examine the implications of both velocity ratio and jet-to-jet separation on its near-field flow dynamics, through the use of both laser-induced fluorescence (LIF) and digital particle image velocimetry (DPIV) techniques.

II. EXPERIMENTAL SETUP

A. Experimental facility and jet apparatus

The present experiments were conducted in a closed-loop low speed water tunnel facility, similar to an earlier study conducted by the authors (New and Zang, 2015). The free-stream flow was conditioned through three layers of fine screens and a 4:1 contraction chamber before entering the test section with an internal dimension of 450 mm (W) × 600 mm (H) × 1100 mm (L). Twin jet flows were produced from a pair of 360 mm long straight cylindrical tubes with a circular jet exit of D = 20 mm diameter each. Water was first channeled from the back end of the water tunnel into the middle compartment of an overhead water tank by a small centrifugal pump from which it then divided equally into two side compartments and flowed through the jet apparatus before exhausting into the

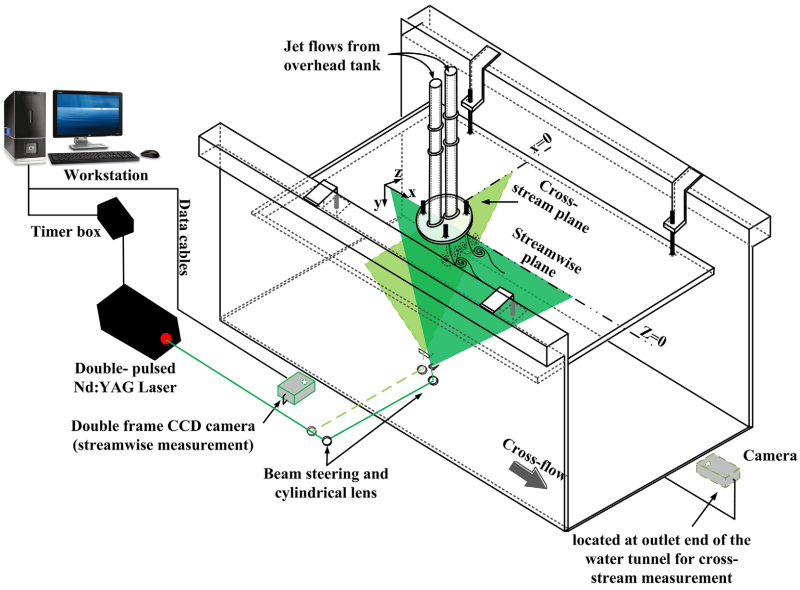

FIG. 1. Schematics of the experimental arrangements used in the present study.

cross-flow. The use of a three-compartment overhead water tank helped to minimize the pulsating effects from the pump, as well as to sustain a constant hydrodynamic pressure head that drove the jet flows. Moreover, the jet volume flow rates were monitored through two separate electromagnetic flowmeters with an uncertainty level of ±0.5% and the different velocity ratios were achieved by carefully adjusting two separate needle valves.

Figure 1 shows the present experimental arrangements around the test section, where a 440 mm (W) × 815 mm (L) Plexiglas flat plate with a round leading-edge was located below the free water surface. The flat plate was firmly secured to the test-section by bolting it to four brackets fixed onto the two top ledges of the test section. Different circular plugs were fitted into the flat plate through a 100 mm diameter circular opening to accommodate either a SJICF or a parallel TJICF configuration, such that both the jet exits and circular plugs remained flushed with the flat plate surface. Flexible rubber hoses were used to complete the jet flow circuit by connecting them from the needle valve exits to the two cylindrical pipes. Three different separation distances (s) of s/D = 1.5, 2, and 3 were considered here. In the present study, the cross-flow velocity was kept constant at U_∞ = 28 mm/s and its turbulence intensity level within the measurement region was approximately 2.6%. The velocity ratios used here were $r = U_j/U_\infty$ = 2, 4, and 6 (where U_j is the time-averaged jet velocity over the jet exit area), corresponding to jet Reynolds numbers of Re_D = 1120, 2240, and 3360, respectively.

Figure 2 describes the set of axes defined for the present experimental measurements, where the Cartesian coordinates x, y, and z align with the horizontal (i.e., streamwise), vertical, and lateral directions with respect to the cross-flow direction, with the origin coinciding with the jet exit centre of the SJICF. As such, the distance from the flat plate leading-edge to the origin was 285 mm, which gave rise to a cross-flow boundary layer thickness of $\delta \approx 1.1D$ at the origin, as determined from the DPIV measurements. Since the use of a round leading-edge was intended to provide a smooth transition for the cross-flow, it also promoted boundary layer growth. Nevertheless, the cross-flow boundary layer is expected to be laminar still, despite that it is slightly thicker than that predicted by Blasius solution. In addition, a ξ-axis is defined to be the mean streamline from the jet exit centre and thus represents the mean deflected jet trajectory. A number of studies have already used the mean streamline to map out the mean jet trajectories successfully, such as Yuan and Street (1998), Muppidi and Mahesh (2005), New *et al.* (2006), and Lim *et al.* (2006). In the present investigation, deflected jet half-widths ($d_{1/2}$) were determined from the DPIV measurements along the ξ-axis.

B. Laser-induced fluorescence and digital particle-image velocimetry techniques

Both LIF and DPIV techniques were employed to capture qualitative and quantitative information on the flow fields and their experimental arrangements were largely similar, as shown in Fig. 1. Illumination from thin laser sheets along the measurement planes was produced from either a 2W

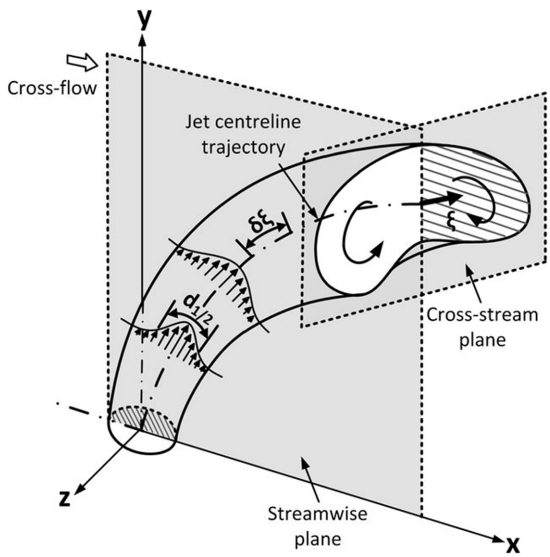

FIG. 2. Definition of the coordinate systems in the present JICF study.

continuous wave 532 nm laser or 200 mJ/pulse double-pulsed 532 nm Nd:YAG laser with beam-steering and sheet-forming optics for LIF and DPIV experiments, respectively. Note that two-dimensional visualization and measurements were taken along both streamwise and cross-stream planes, as indicated in Fig. 2. To differentiate between the two independent jets during LIF visualizations, two different fluorescent dyes were premixed into the overhead water tank prior to the experiments, with fluorescein disodium and Rhodamine B used in each jet. Under the excitation of the laser, they fluoresced in green and orange colours, respectively. The addition of the fluorescence dyes was estimated to increase the water density by 0.025% and hence their effects can be neglected. A digital single-lens-reflex camera with an f 1.8, 50 mm lens was remotely controlled by a workstation to capture 1920 px × 1080 px video recordings of the LIF visualizations at 30 frames-per-second (fps). At least 30 s of video recording was captured for each test configuration and still images were subsequently extracted for analysis during the study.

On the other hand, 20 μm polyamide seeding particles were seeded uniformly into the water tunnel for DPIV measurements. Reflected light from the particles was captured by a Dantec Dynamics FlowSense 2M/E double-frame camera with a CCD array size of 1600 px × 1200 px and a total of 1000 image pairs were collected at a sampling rate of 15 Hz without any preferences to the exact phase of the flow fields. The time-interval (Δt) between the two images within an image pair varied from 2.4 ms to 8 ms, such that particle shifts were no more than 20% in the final interrogation window for all the different velocity ratios and measurement planes used. The particle images were subsequently subjected to a two-pass multi-grid cross-correlation algorithm with global and local validation schemes, where the initial and final interrogation window sizes were 128 px × 128 px and 32 px × 32 px, respectively, with 50% area overlaps in both horizontal and vertical directions.

The actual physical sizes of the measurement windows are approximately 200 mm × 150 mm in the streamwise plane and 300 mm × 225 mm in the cross-stream plane, respectively. The DPIV experiments were carried out according to the guidelines detailed in Keane and Adrian (1992). This leads to an uncertainty of approximately 1.3% on the velocity vectors from DPIV measurements (Keane and Adrian, 1992 and Westerweel, 1997) and approximately 3.5% on the derived vorticity $\vec{\omega} = \nabla \times \vec{u}$ (Moffat, 1988 and Raffel *et al.*, 2007). Mean jet exit velocity profiles for the single and twin JICF configurations were demonstrated in an earlier study to be mostly parabolic across different velocity ratios and separation distances [refer to Fig. 2 in the study by New and Zang (2015)]. Additionally, the peak mean jet exit shear layer turbulence intensity level for the single jet configuration is approximately u'/U = 0.1, while that of the twin-jet configuration increases gradually from approximately u'/U = 0.12 to 0.14 when the separation distance was reduced.

III. RESULTS AND DISCUSSIONS

For consistency and ease in the following discussions, nomenclatures used to differentiate between the different measurement planes should first be clarified. For instance, the streamwise plane taken along one of the jet exit centres will be termed the "jet plane," whereas that along the centre between two jet exits will be referred to as the "symmetry plane." Cross-stream planes, on the other hand, refer to planes across the cross-flow direction and will correspond to longitudinal distances downstream of the origin.

A. Streamwise flow developments along jet plane

To begin with, Fig. 3 first shows the instantaneous LIF visualization images taken along the jet planes for the SJICF and parallel TJICF at different velocity ratios and separation distances. Qualitative flow changes due to variations in both velocity ratios and separations can be directly observed from the flow visualization results. As depicted in Fig. 3(a), the flow behaviour of the SJICF demonstrates good qualitative agreements with the results obtained in previous studies, such as Fric and Roshko (1994) and Kelso *et al.* (1996). For instance, leading-edge and lee-side vortices form regularly in a daisy-chained pattern along the jet shear layer after the jet exhausts into cross-flow. As the velocity ratio increases from r = 2 to 6 [from Fig. 3(a), (i)–(iii)] and the jet momentum increases, the jet penetrates deeper into the cross-flow with correspondingly higher jet trajectories. In addition, formations of leading-edge and lee-side vortices move progressively closer to the jet exit with higher velocity ratios due to the decrease in the initial jet boundary layer displacement thickness, which is inversely proportional to jet Reynolds number (Becker and Massaro, 1968 and Schlichting and Gersten, 2000). On the other hand, Figs. 3(b)–3(d) show the visualized parallel TJICF flow fields taken along the jet planes, located at z/D = −0.75, −1, and −1.5 for s/D = 1.5, 2, and 3 separation distances, respectively. Note that the deflected jets visualized here were premixed with Rhodamine B dye while the adjacent parallel jets were premixed with fluorescein disodium dyes. Besides the general resemblance with a SJICF, such as regular formations of the leading-edge and lee-side vortices, mutual entrainment of jet fluids can be clearly discerned with the presence of green-coloured dyes from the adjacent parallel jets, regardless of the velocity ratio and separation distance. It can be observed that the location at which the two deflected parallel jets begin to interact with each other shifts higher above the jet exit as well as further downstream, when the velocity ratio and separation distance increase, respectively. Moreover, entrained fluid from the adjacent parallel jet can be observed to mainly concentrate and convect along the lee-side of the in-plane jet, indicating significant near-field interactions between the two parallel CVPs right from their initiations onwards.

Closer examinations of Figs. 3(b)–3(d) shed some light upon the mutual jet interactions that occur at different velocity ratios and separation distances. For instance, it can be discerned that near-field interactions and entrainment become more significant at higher velocity ratios and/or smaller separation distances. Furthermore, more flow activities and hence more dye highlighted regions at the lee-side of the parallel TJICF as compared to the SJICF can be also observed, especially at s/D = 1.5 and 2.0 separation distances. Interestingly, these heightened flow activities at the jet lee-sides seem to encourage interactions between the deflected jet and the cross-flow boundary layer for s/D = 1.5 at r = 2, as shown in Fig. 3(b),

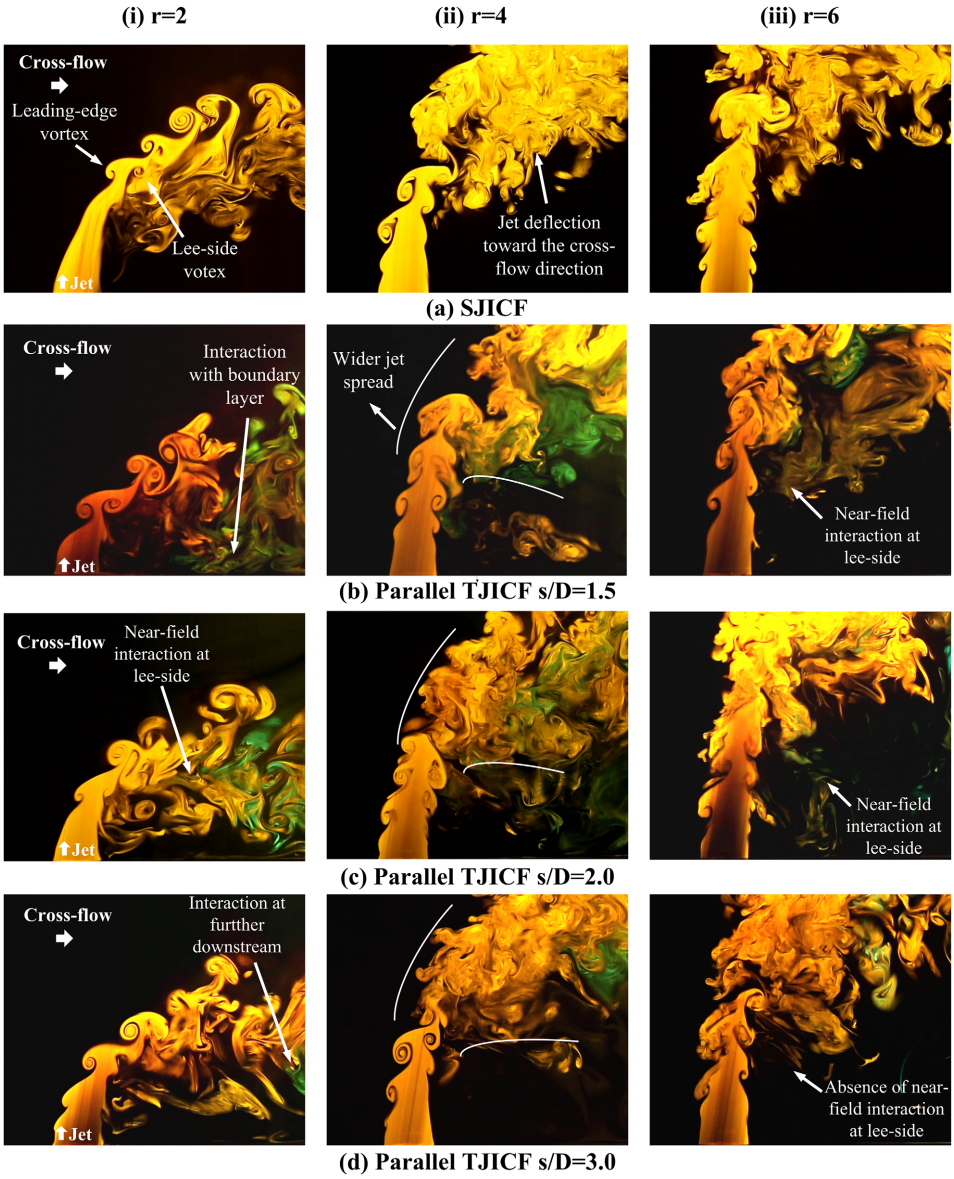

FIG. 3. Instantaneous laser-induced fluorescence images of (a) SJICF, (b) parallel TJICF s/D = 1.5, (c) parallel TJICF s/D = 2.0, and (d) parallel TJICF s/D = 3.0 at r = 2 to 6, along the streamwise jet plane.

(i). Last but not least, it is also noteworthy that the formations of the leading-edge and lee-side vortices are generally closer to the jet exit for parallel TJICF in Figs. 3(b)–3(d), which support observations of higher initial turbulence intensity levels in the twin jet shear layers.

Next, profiles of mean vertical velocity component (i.e., v) extracted at downstream locations between x/D = 0 to 4 are presented in Fig. 4 to provide a quantitative comparison between the SJICF and parallel TJICF. A number of earlier studies have presented such vertical velocity profiles to better reveal the developments of a JICF, take for instance Andreopoulos and Rodi (1984), Sherif and Pletcher (1989), and New *et al.* (2006). This is especially the case along both jet and symmetry planes, where the velocity components along x- and y-directions remain dominant within the near-field.

Hence, it will be useful to first identify the characteristics of the mean vertical velocity component profiles for the SJICF as a matter of benchmarking and Fig. 4(a) shows its streamwise development at r = 2 (i.e., annotated by empty symbols). Note that results obtained by New *et al.* (2006) at r = 2.3 have also been included for comparisons (i.e., annotated by solid and dotted lines). The general distributions of these velocity profiles along the y-direction obtained from the present study can be observed to be consistent with those reported earlier by New *et al.* (2006), where the jet incurs rapid reductions in its vertical velocity component magnitudes. Moreover, two velocity peaks can also be observed immediately downstream of the jet exit at x/D = 1. With a higher magnitude along the velocity profile, the primary peak "P" is associated with the deflected jet core. It can be seen to displace further away from the jet exit surface with increasingly smaller magnitudes, as the deflected jet gradually aligns itself in the cross-flow direction at further downstream locations. As such, a collection of these peaks along the streamwise direction will map out the approximate jet trajectory in the near-field. On the other hand, the secondary peak "S" can be attributed to the vertical velocity component induced by the CVP along its jet plane, as it initiates close to the jet exit and develops beneath the deflected jet core (Kelso *et al.*, 1996; Yuan *et al.*, 1999; and Lim *et al.*, 2001). Similar to the primary peak,

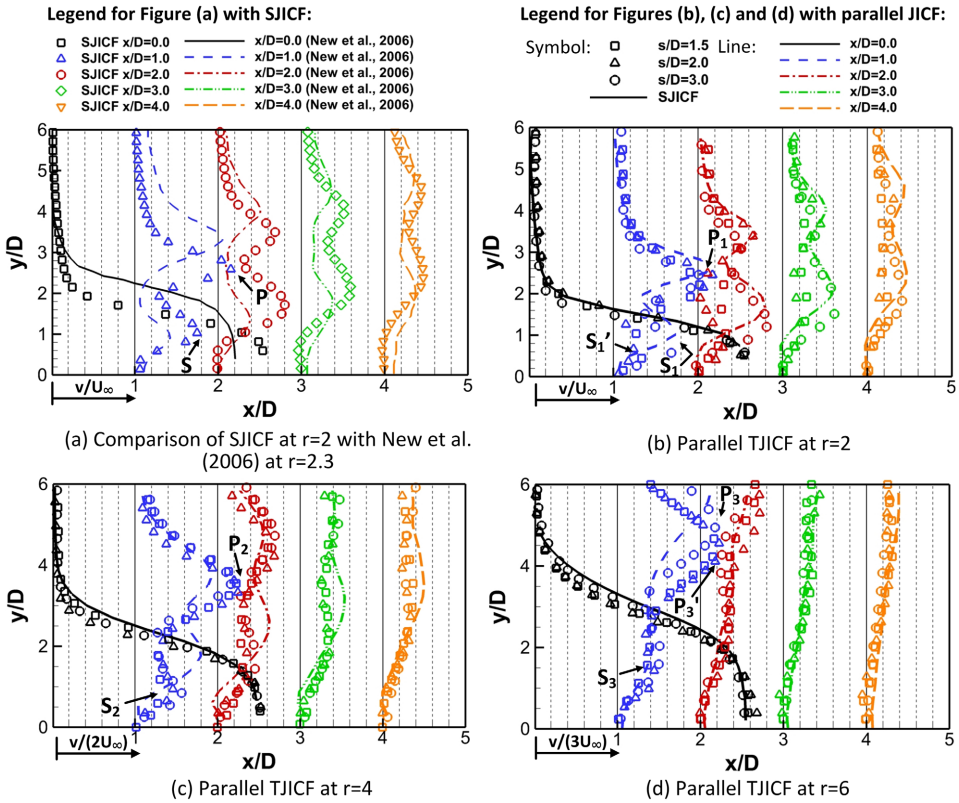

FIG. 4. Streamwise development of the mean vertical velocity component profiles from x/D = 0 to 4 along the jet plane, for both SJICF and parallel TJICF at r = 2 to 6. Symbols are the same for (b)–(d).

the secondary peak location continues to move further away from the jet exit surface at increasingly further downstream locations.

Corresponding velocity profiles extracted for the parallel TJICF at s/D = 1.5, 2, and 3 are shown in Figs. 4(b)–4(d), respectively, where the effects of the velocity ratio and separation distance are apparent. As can be inferred from Fig. 4(b) at r = 2, the magnitude of the secondary peak (i.e., S_1) associated with s/D = 3 separation distance is approximately 1.5 times greater and located relatively higher above the jet exit surface than that (i.e., S_1') with s/D = 1.5. Note that since the secondary peaks for s/D = 1.5 and 2 remain relatively comparable in both magnitude and location at r = 2, only s/D = 1.5 scenario is marked to highlight the differences here. As the separation distance decreases, CVPs produced by the two parallel jets will interact with each other earlier in their formations (i.e., more details on this will be presented later), which could lead to smaller induced vertical velocity magnitudes. Such mutual interactions will be more prominent at lower velocity ratios due to two reasons—firstly, lower CVP strengths make them more sensitive towards mutual interactions and secondly, deflection of the jet cores over a shorter downstream distance means that the two CVPs from parallel TJICF form and interact earlier downstream, leading to more pronounced differences in the v-velocity component (Karagozian, 1986). If that is the case, the effects of separation distance on the secondary peak behaviour are expected to be more subdued as the velocity ratio increases to r = 4 and 6. This is certainly the case if one considers the secondary peaks S_2 and S_3 in Figs. 4(c) and 4(d), respectively, though minor discrepancies can be discerned with the smallest magnitudes associated with s/D = 1.5. These secondary peaks (i.e., S_1, S_1', as well as S_2, and S_3 at higher velocity ratios) observed in parallel TJICF move away from the jet exit surface at increasingly downstream locations, similar to that of a SJICF (i.e., S). Moreover, the associated vertical velocity magnitudes decrease notably within the near-field due to the relatively rapid decay of the individual CVP vortex strengths, which results directly from the mutual annihilation of the inner vortices. Mean vorticity results to be presented later in Figs. 9 and 10 confirm this by showing that the annihilation of vorticity takes place quickly in the near-field region, which would in turn reduce the vertical velocity components (more details on the CVP interactions will be presented in Secs. III C–III E).

Interestingly, the trends are reversed for the primary peaks as the velocity ratio increases. As can be seen in P_3 and P_3' in Fig. 4(d) that correspond to the primary peaks associated with s/D = 3 and s/D = 2 (and similarly s/D = 1.5), respectively, there exist increasing deficits in the vertical jet momentum for parallel TJICF with smaller separation distances. Since the primary peaks are associated with the jet core trajectories, it can be inferred that the jet penetrates less into the cross-flow before incurring significant deflection in the near-field for s/D = 1.5 and 2 parallel TJICF at r = 6. Nevertheless, the jet trajectories remain comparable at the three different separation distances for the lower velocity ratio of r = 2. Meanwhile, it is worthwhile to note that the near-field trajectories of the parallel TJICF as indicated by the primary peaks along the streamwise direction are lower than that of the SJICF at any specific velocity ratio. This is in good agreement with the observations made by Toy *et al.* (1993) on parallel TJICF and Holdeman *et al.* (1997) on parallel multiple JICF. In particular, Holdeman *et al.* (1997) concluded that the use of parallel JICF was equivalent to lowering the velocity ratio of the JICF.

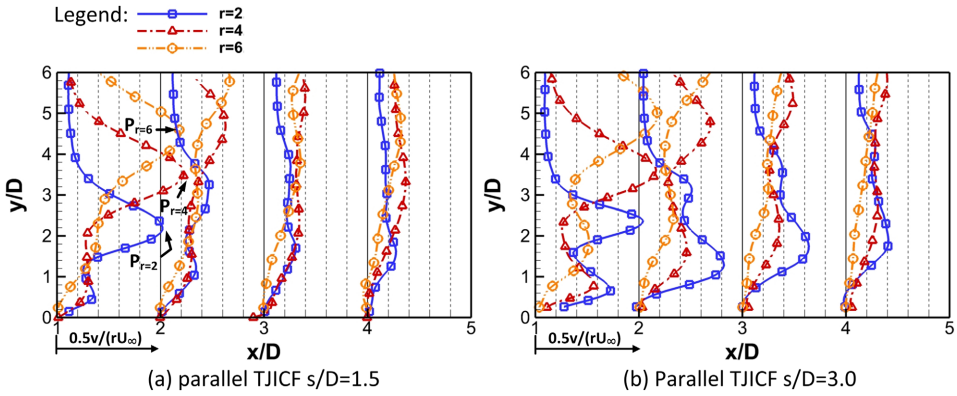

FIG. 5. Scaling of mean vertical velocity based on velocity ratio along the jet plane from x/D = 1 to 4 downstream locations with (a) s/D = 1.5 and (b) s/D = 3.0.

To examine how the vertical velocity component scales with the velocity ratio at a specific separation distance and downstream location, Fig. 5 shows the scaling of the mean vertical velocity profiles by "0.5r" for x/D = 0 to 4 locations, with results for three different velocity ratios all collapsed into a single figure to ease comparisons. "0.5r" is used to allow better scaling of the velocity profiles within the limited space, as well as to prevent data cluttering. The figure shows that the trends remain consistent to those observed in the normalized mean vertical velocity profiles in both Figs. 4 and 7. Interestingly, the primary peak magnitudes of the scaled mean vertical velocity profiles are largely comparable with one another with minor discrepancies, regardless of the exact velocity ratio or downstream location. Furthermore, it can be observed that at higher velocity ratios where smaller jet deflections and greater upwards momentums exist, the peak magnitudes tend to be greater than those associated with lower velocity ratios [see $P_{r=6}$, $P_{r=4}$, and $P_{r=2}$ in Fig. 5(a)]. On the other hand, the scaled secondary peaks exhibit more significant differences as the velocity ratio increases from r = 2 to 6.

Previous studies have indicated that the entrainment of the cross-flow fluid contributes significantly towards the characteristic deflection of a JICF towards the cross-flow direction (Pratte and Baines, 1967; Smith and Mungal, 1998; and Yuan *et al.*, 1999), which subsequently determines the trajectory of a JICF. Hence, in an attempt to understand the lower parallel TJICF trajectories within the context of jet entrainment behaviour, the jet half-widths along the jet centre axis (i.e., ξ-axis) are determined and shown in Fig. 6. Recall that the ξ-axis aligns with the mean jet streamline originating from the

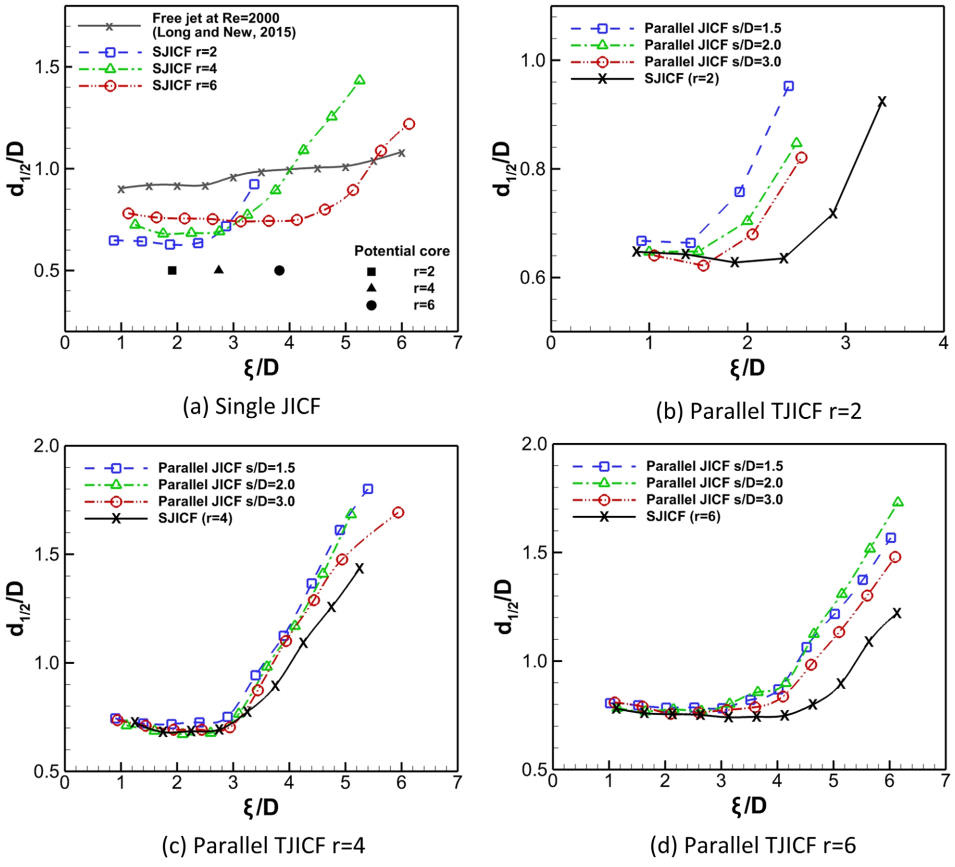

FIG. 6. Near-field jet half-widths ($d_{1/2}$) determined along the ξ-axis for the SJICF and parallel TJICF at r = 2 to 6.

jet exit centre. Hence, line segments normal to the ξ-axis could first be found with reference to the mean jet streamline from ξ/D = 1 to 6 at ξ/D = 0.5 intervals, along which jet half-widths were then extracted from the mean velocity vector fields. Definition of jet half-width here adheres to the conventional definition as the distance away from the mean jet streamline where the jet velocity decays to half that of the maximum jet velocity. Savory and Toy (1991) and Toy *et al.* (1993) compared the jet half-widths between single and two side-by-side JICF (i.e., parallel TJICF) at relatively far-field regions from x/D = 10 to 30 and noted larger jet half-widths along the jet plane for the side-by-side configuration. Nevertheless, they only presented results for a single velocity ratio and separation distance (i.e., r = 8 and s/D = 5), which reveal limited information. Therefore, the present results aim to shed more light upon the impacts of velocity ratio and separation distance upon the jet spread of parallel TJICF along the jet trajectories.

Figure 6(a) shows the jet half-width distributions for the SJICF at three different velocity ratios. The half-width growth of a single free jet at Re_D = 2000 is included as a reference (Long and New, 2015). Though the jet exit Reynolds number of their experiments is different from the present study, it clearly illustrates the different mixing behaviours of a single free jet and a SJICF. In the near-field, while the free-jet half-width grows almost linearly with the downstream distance for the free jet, that of the SJICF sees abrupt increases at approximately x/D = 2.4, 3, and 4 downstream for r = 2, 4, and 6, respectively. It should be mentioned that the mean jet centre velocity becomes comparable to the cross-flow velocity shortly after its trajectory aligns with the cross-flow at r = 2 and therefore the jet half-width was only determined up to ξ/D = 3.5. Based on large-eddy simulations on a SJICF, Yuan *et al.* (1999) observed that a significant amount of the cross-flow fluid would be entrained by the jet at a position where notable deflection of the jet column began. Since the growths of the jet half-width and hence the jet spread are directly related to the entrainment of the cross-flow fluid, and that the jet deflects more rapidly beyond the jet potential core region (Pratte and Baines, 1967), it may be argued that the position of the sharp "deflection" is expected to be at some downstream distance in close proximity of the jet potential core, relatively invariant to changes in the velocity ratio. Subsequently, the potential core lengths of the SJICF were calculated according to the definition used in the study by Pratte and Baines (1967) and included into Fig. 5(a), which can be seen to provide clear support to the preceding argument and hence the observations made by Yuan *et al.* (1999) on the near-field entrainment.

On the other hand, Figs. 6(b)–6(d) show that parallel TJICF have considerably larger overall jet half-widths than the SJICF for all different velocity ratios and separation distances, which is in good agreement with the results of Toy *et al.* (1993). Take for instance, the jet half-width of the parallel TJICF at r = 6 and s/D = 1.5 is approximately 30% greater than that of the SJICF. It will be useful to recall from the earlier LIF flow visualization images that with relatively small separation distances, interactions between the parallel TJICF in the near-field allow mutual entrainment of the jet fluids, which are also likely to promote entrainment of the cross-flow fluid into the jets themselves. This will then explain the larger jet half-widths for the parallel TJICF. Similar to the mean vertical velocity component profile results presented earlier, the separation distance is most influential at r = 2 where differences between the jet half-widths of the three separations become significant. In contrast, the jet half-widths become comparable as the velocity ratio increases to r = 4 and 6 within the measurement range. At this point, it is not clear if the effects on the jet half-widths due to separation distances will become significant at downstream locations beyond the present measurement range at higher velocity ratios. Nevertheless it can be deduced from the results presented so far that the near-field developments of the parallel TJICF are more sensitive to the separation distance at lower velocity ratios.

B. Streamwise flow developments along symmetry plane

For parallel TJICF configurations, they all share a common symmetry plane that is aligned along the centre between the twin jet exits (x/D = 0) and parallel to the cross-flow. More importantly, this plane is where the twin jets are expected to encounter each other eventually. As far as the authors understand, only a few studies in the past have examined the flow behaviour along this particular plane. Similar to jet-plane results shown in Fig. 4, the mean vertical velocity component profiles at different streamwise locations are presented in Fig. 7, with corresponding results for the SJICF included for comparisons. It should be noted that the symmetry and jet planes are identical for a SJICF configuration.

At a downstream location of x/D = 1 at r = 2, negative vertical velocity magnitudes are observed between y/D = 1 and 2 above the jet exit surface, as indicated in Fig. 7(a). This indicates the presence of downward flow regions for all three different velocity ratios and separation distances. Andreopoulos and Rodi (1984) also detected a region of downward flow in a SJICF close to the jet exit and they postulated that it was induced by a bound vortex present in the wake region of the SJICF. However, they did not resolve the origin of the bound vortex due to limitations in their measurements. In the present study, however, the downward velocity along the symmetry plane of the parallel TJICF here appears to be induced by vortical structure arising from interactions between the two parallel jets, where it could be similar to the bound vortex postulated by Andreopoulos and Rodi (1984).

A glimpse of the structure can be seen in the instantaneous vorticity field maps in Fig. 8(a), (i) and (ii) for parallel TJICF with smaller separation distances at r = 4, where it is located at approximately x/D = 1.2 and y/D = 0.8. Having a positive vorticity and hence anti-clockwise rotation, the vortical structure will induce a downwards-acting velocity component in the region. Moving further up from the jet exit surface at x/D = 1, only a single velocity peak is detected with s/D = 1.5, regardless of the velocity ratio (as indicated by "SS," "SS_1," and "SS_2" for r = 2, 4, and 6, respectively). Interestingly, the single peak (for instance, the peak "SS") is located approximately in the middle of the primary and secondary peaks associated with the SJICF. Along the symmetry plane, any upward momentum is supplied from the twin interacting jets, and hence further increasing their separation will see a decrease in the

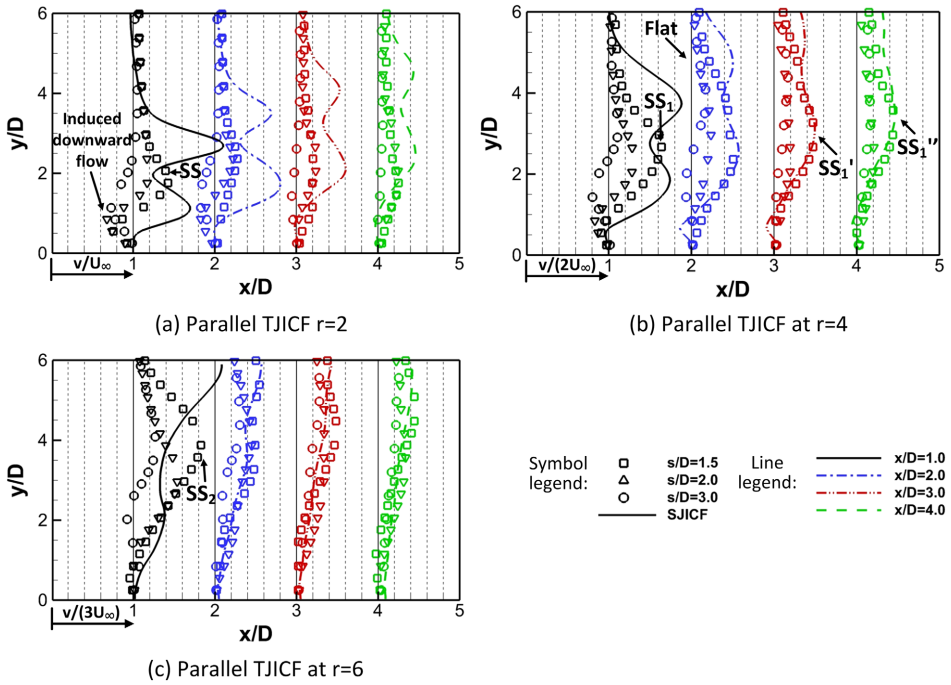

FIG. 7. Streamwise development of the mean vertical velocity component profiles from x/D = 0 to 4 along symmetry plane for the parallel TJICF at r = 2 to 6. Symbols are the same for (a)–(c).

magnitude of the single velocity peak. However, it is noteworthy that velocity peaks are absent at r = 2 and s/D = 3, meaning that the mutual interactions along the symmetry plane are considerably limited in the near-field. Conversely, the v-velocity profile becomes remarkably comparable to a SJICF at r = 6 and s/D = 1.5 along the symmetry plane from x/D = 2 onwards, which implies that as the parallel TJICF impinges upon each other early along the symmetry plane at the smallest separation, the interacting jets develop quickly into a combined JICF that is comparable to SJICF. In fact, the cross-stream measurement results presented later will lend more support to this observation along the symmetry plane. Moving further downstream to x/D = 3 and 4, the variations in the v-velocity profiles become considerably more gradual. As the figure shows, the

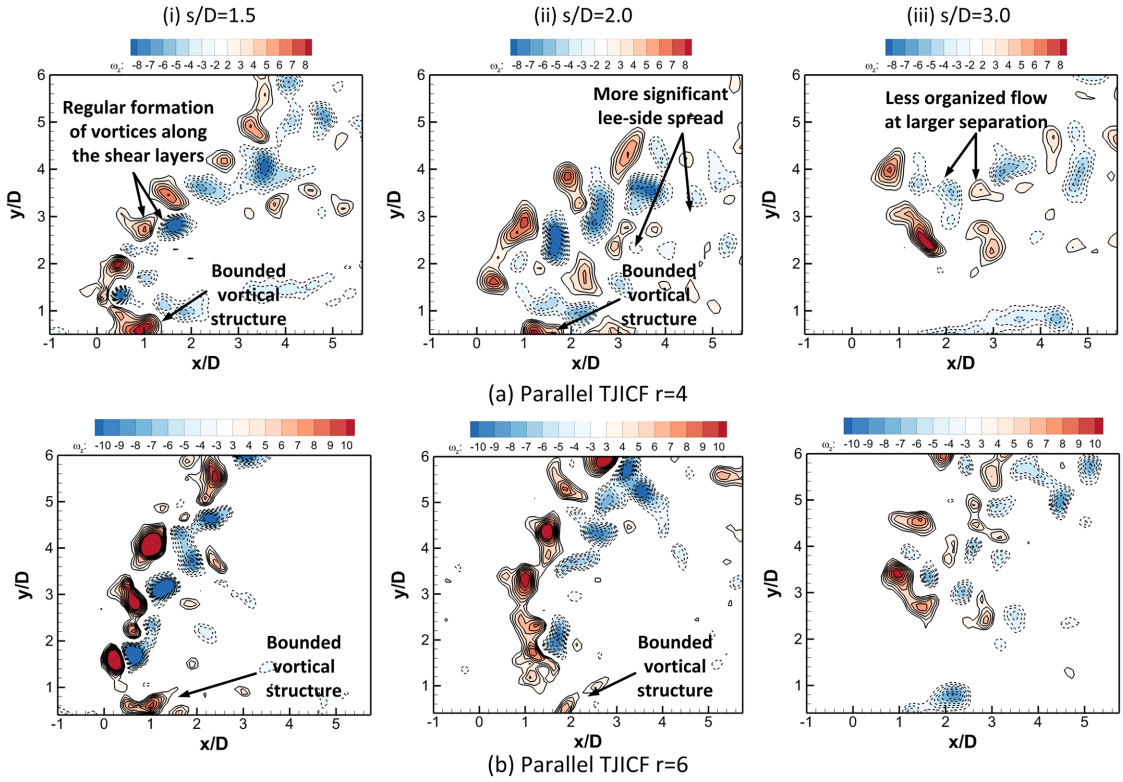

FIG. 8. Impingement of the jet shear layers along the symmetry plane for the parallel TJICF with three different separations (i.e., s/D = 1.5, 2.0, and 3.0) at (a) r = 4 and (b) r = 6.

peak associated with s/D = 1.5 parallel TJICF at r = 4 (i.e., denoted by square symbol) moves further away from the jet exit surface as the twin jets convect downstream from x/D = 3 (i.e., P_1) to 4 (i.e., P_1'), while the reduction in magnitude is minor. Considering that the twin jets begin to interact almost immediately downstream of the jet exit (as will be seen in Figs. 9 and 10 later) and the two individual CVPs merge quickly into a single CVP at approximately x/D = 3, the vertical velocity along the symmetry plane would be primarily induced by the outer pair of vortices (i.e., the merged CVP). And as the strength of the outer vortices decays slowly with downstream distance, it is reasonable to expect the reduction in the peak magnitude to be very gradual.

However, an interesting question is then raised as to how the jet shear layer vortices will behave, if the parallel TJICF indeed becomes single-JICF like in the near-field. To answer this question, one has to refer to Fig. 8, where relatively coherent and organized vortices are observed with smaller separation distances s/D = 1.5 and 2.0, but are absent as the separation increases to s/D = 3, for both velocity ratios of r = 4 and 6 along the symmetry plane. In particular, the rows of opposite-signed vortices are arranged in an alternate fashion for s/D = 1.5 and 2.0 separation distances and deflect towards the cross-flow direction, bearing the trademarks of the daisy-chained leading-edge and lee-side vortices seen in SJICF. On the other hand, the flow becomes significantly less organized at s/D = 3 separation distance and the coherent vortices are no longer discernible, as shown in Figs. 8(a) and 8(b), (iii). Furthermore, the figure shows that bounded vortical structures are produced at smaller separation distances of s/D = 1.5 and 2.0, but absent as the separation distance is increased to s/D = 3, regardless of the exact velocity-ratio. Such behaviour could be attributed to the recovery of the cross-flow boundary layer at the lee-side of the parallel TJICF. Since the exhausting twin jets act like two obstacles to the cross-flow at a sufficiently large separation distance, the cross-flow boundary layer will be displaced around the both sides and recover at the lee-side of each jet at some downstream distance (Fric and Roshko, 1994). In that case, the displacements of the boundary layer from both jets will interact along the flow-field symmetry plane and conceivably produce the observed negative vorticity regions. On the other hand, as the separation distance becomes smaller, the cross-flow boundary layer will be more likely to be displaced around and recover at the lee-side of the twin jets as if they resemble one single but larger obstacle. As such, the flow behaviour along the symmetry plane will be very different from that observed for larger separation distances, which agrees well with the outcomes depicted in Fig. 8 here.

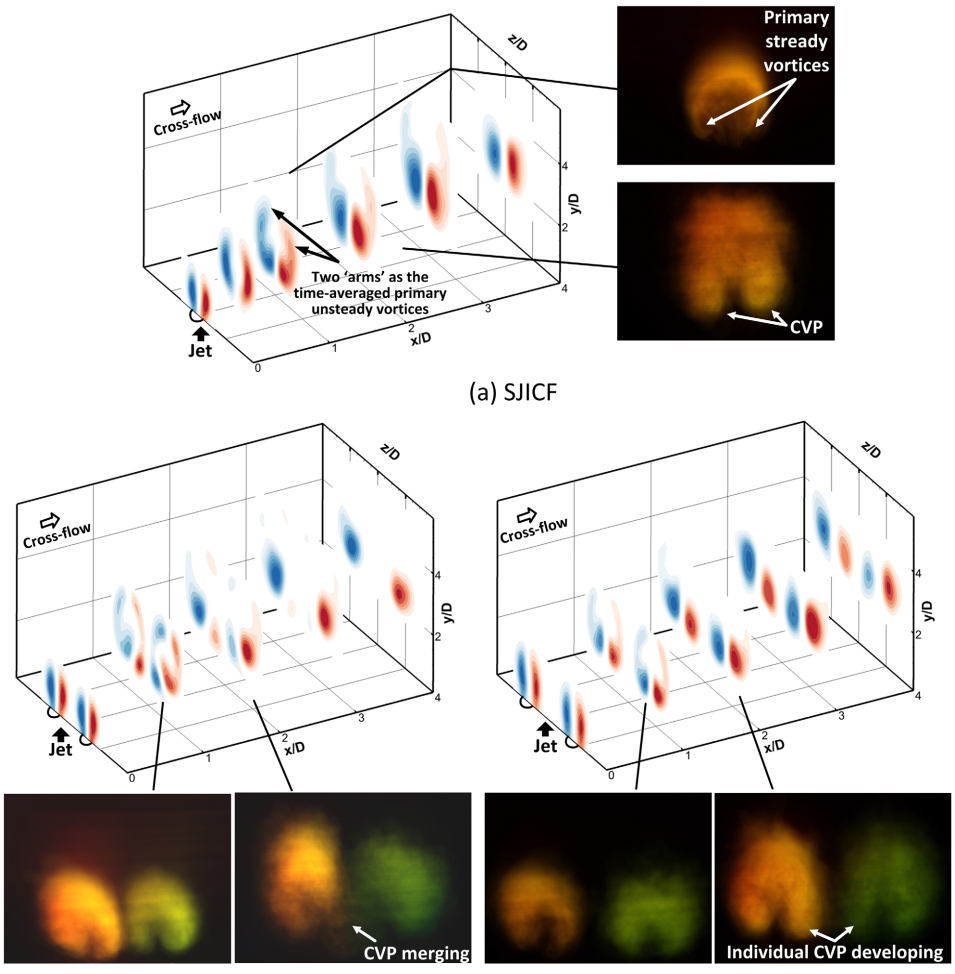

FIG. 9. Mean cross-stream DPIV vorticity results and LIF visualizations of near-field formations of and interactions between the two CVPs for (a) SJICF, (b) s/D = 2, and (c) s/D = 3 parallel TJICF at lower velocity ratio of r = 2.

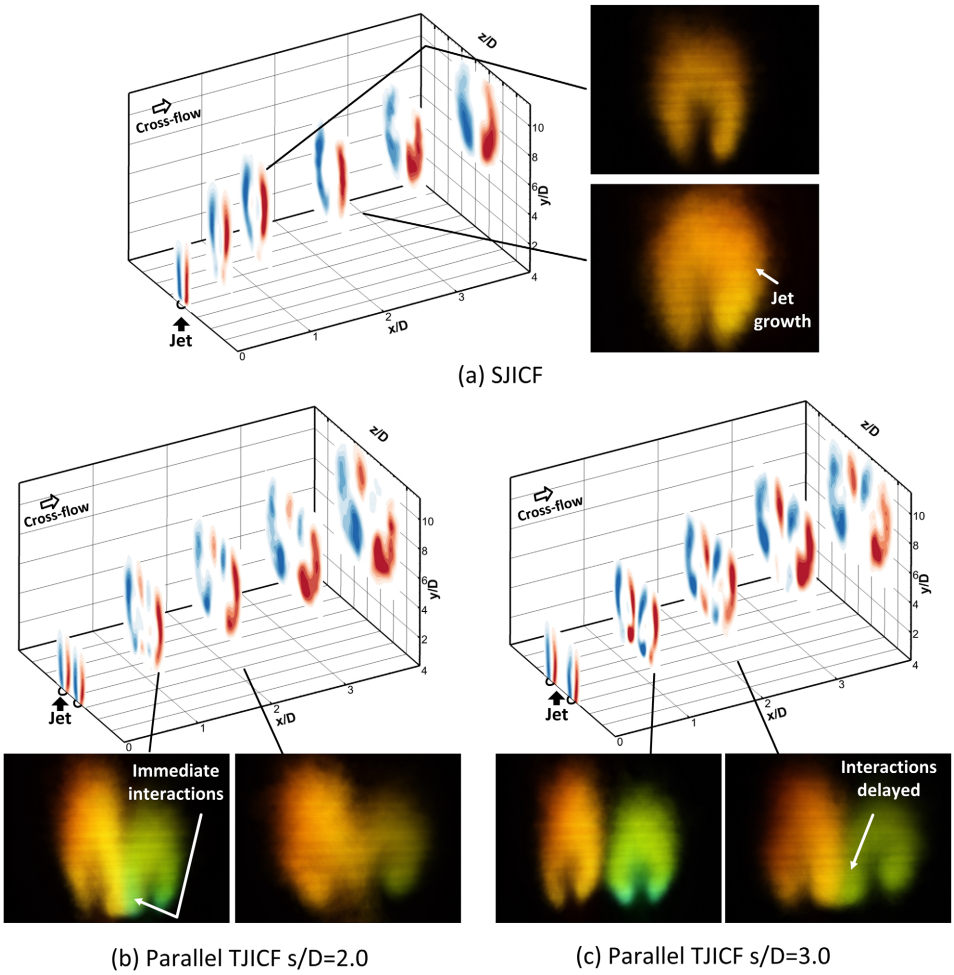

FIG. 10. Mean cross-stream DPIV vorticity results and LIF visualizations of near-field formations of and interactions between the two CVPs for (a) SJICF, (b) s/D = 2, and (c) s/D = 3 parallel TJICF at higher velocity ratio of r = 6.

The presence of the large-scale coherent structures at sufficiently small separation distances is likely to further enhance the mixing between the parallel TJICF with cross-flow fluid along the symmetry plane, which would explain the better cooling effects recorded by Holdeman and Walker (1977) along the symmetry plane by using more closely spaced multiple JICF arranged in parallel. Last but not least, in order to better control the mixing levels along the symmetry plane, it may be worthwhile to investigate the vorticity contributions from each of the both parallel jets and compare them with the resulting organized motion of the large-scale coherent structures.

C. Developments of counter-rotating vortex-pairs

Another key aspect governing the near-field flow dynamics of parallel TJICF relates to the interactions between the CVPs. The developmental processes of the CVP structure and its associated vorticity from a SJICF have been well studied and discussed, starting from the jet exit till the far-field region. Readers are advised to refer to the reviews on JICF for details [take for instance, Mahesh (2013) and Karazogian (2014)]. Furthermore, it has been noted by Smith and Mungal (1998) that a CVP structure could be best described from its mean flow characteristics. Therefore, the present discussions will focus on the near-field transitional process of the CVP structures associated with parallel TJICF as observed from their time-averaged flow fields. The nomenclatures describing the various vortical structures associated with the cross-stream DPIV measurement adhere to those used in New *et al.* (2003). For instance, the primary steady vortices refer to the primary CVP flow features and the primary unsteady vortices are manifestation of the leading-edge vortices crossing the 2D cross-stream measurement plane.

Figure 9 shows the mean cross-stream DPIV vorticity results and LIF visualizations from x/D = 0 to 4 for SJICF and parallel TJICF at s/D = 2 and 3 with r = 2. In addition to the DPIV results, mean LIF flow images at x/D = 1 and 2 locations are also included in the figure to provide direct visual observations on the effects of separation distance. A total of 512 still images extracted from the video recordings were subjected to equally weighted linear image averaging process to produce the mean LIF results. From the mean vorticity results of the SJICF shown in Fig. 9(a), the pair of jet shear layers observed at x/D = 0 quickly manifests into primary steady vortices (i.e., the primary CVPs). Furthermore, the two "arms" extending upwards from the primary steady vortices and symmetric about symmetry plane correspond to the time-averaged "footprints" of the primary unsteady vortices (i.e., leading-edge vortices). Since the leading-edge vortex loops regularly form and travel across the cross-stream measurement planes, they manifest as the jet shear layers in the mean vorticity results (Haven and Kurosaka, 1997 and New *et al.*, 2003). More importantly, the CVP formation appears to have

completed by x/D = 4 location, where unsteady primary vortices have largely disappeared from the mean vorticity results and the cross-stream flow field becomes dominated by a distinct pair of CVPs. Both Karagozian (1986) and Fric (1990) noted rapid CVP formations from their analytical model and experimental measurements, respectively.

Moving on to the parallel TJICF configuration, interactions between the CVPs are discernible immediately downstream of the jet exits at smaller separation distance of s/D = 2, as shown in Fig. 9(b). With a smaller separation distance, the spatial confinement between the two CVPs quickly becomes the limiting factor to their growths along the symmetry plane, as shown in the mean LIF images taken at x/D = 2 in Fig. 9(b). Due to their proximity, the pair of inner vortices (i.e., vortices closest to the symmetry plane) first experiences increases in their vortex strength as they interact mutually within the confined space, which can be clearly observed at x/D = 1 in Fig. 9(b). This is shortly followed by the annihilation of the opposite-signed inner vortices, where their mutual cancellation occurs rather rapidly such that they are no longer visible in the vorticity results from approximately x/D = 4 onwards. Therefore, despite the fact that two jets are actually exhausted into the cross-flow at r = 2, only a single resulting CVP can be observed within a relatively short distance downstream of the jet exits. Moreover, the two outer vortices (i.e., as opposed to the inner ones) are observed not to participate significantly during the annihilation process from the LIF visualizations, and as such it would appear that the resulting single CVP for the parallel TJICF consists of one outer vortex from each jet.

In contrast, it can be readily appreciated from Fig. 9(c) that two distinct CVPs originating from the two parallel jets are formed independently when the separation distance increases to s/D = 3. At this largest separation distance, the mean vorticity results show that the behaviour of each jet is comparable to that of the SJICF, from the point it exhausts from the jet exit to the formation of the CVP. Furthermore, the two pairs of CVPs remain distinct at the furthest cross-stream plane measured in the present study, though weakened vorticity strengths of the two inner vortices suggest that they are likely to cancel each other through mutual interactions eventually due to their opposite-signed vorticities. Note that same vorticity ranges are applied to all SJICF and parallel TJICF configurations here for ease of comparisons.

On the other hand, Fig. 10 shows the near-field interactions and development of the two CVPs at a higher velocity ratio of r = 6, similarly through the mean vorticity maps measured from x/D = 0 to 4 cross-stream planes. At this higher velocity ratio, the CVP requires a longer downstream distance to develop. However, the present range of measurements is able to better highlight the effects of velocity ratio and separation distance upon the dynamics of the CVPs. First, the two CVPs interact shortly downstream of the jet exits and evolve into a single CVP structure from x/D = 4 onwards for both s/D = 2 and 3 separation distances, as can be seen by comparing Figs. 10(b) and 10(c). When the velocity ratio increases, it is logical that the JICF will entrain more cross-flow fluid in the near-field through intensified formation of leading-edge and lee-side vortices close to the jet exit. Hence, a faster growth in the jet width leads to earlier CVP mutual interactions closer to the jet exit. As a result, increasing the velocity ratio is likely to confer similar effects upon the CVP near-field developments as if the separation distance were to be reduced. Furthermore, note that the inner vortices have almost cancelled each other out completely by x/D = 1 location for s/D = 2 separation distance, which indicates that the interactions between the inner vortices possibly take place alongside with their formations.

Although this does not affect the structure of the resulting single CVP, it does influence upon the near-field circulation and entrainment of the parallel TJICF. Additionally, it is interesting to note that the average "footprint" of the primary unsteady vortices remains discernible even after merging of the two CVPs and persists beyond the present measurement window. The existence of the inner pair of primary unsteady vortices suggests that development of the leading-edge vortex loops is less restricted at higher velocity ratios, such that they continue to contribute significantly to the near-field entrainment of the cross-flow fluid for parallel TJICF. After discussing the general topological development of the CVPs for parallel TJICF, it will be useful to take a closer look at the vortical interactions between these CVPs. Figure 11(a) shows the mean vorticity field along the x/D = 2 plane for the parallel TJICF at s/D = 2 and r = 2, where the CVP structures and their mutual interactions can be clearly observed. As mentioned earlier, the coherent structures above the CVPs are time-averaged "footprints" of the transient motions of the primary unsteady vortices crossing the cross-stream plane (Lim *et al.*, 2001). To filter out such transient effects, λ_2-criteria are imposed on the velocity vector field and the result shown in Fig. 11(b). The use of λ_2-criteria is to more precisely differentiate vortex cores from coherent structures in a shear flow (Jeong and Hussain, 1995). The present λ_2-criteria filtered result reaffirm that the term "time-averaged footprint" used in describing these structures is appropriate and that the λ_2-criteria are more appropriate in vortex identification over vorticity here. With reference to the λ_2-criteria filtered results, Fig. 11(d) shows a simplified illustration of the four vortices and their vortex filaments associated with the near-field CVP developments when the separation distance is sufficiently small.

It is worthwhile to note that the use of vortex filament and its associated circulation strength proves to be effective in analysing and explaining the dynamics and development of the CVP structures in a JICF. For instance, Karagozian (1986) provided a kinematic model for a SJICF by considering the jet column as quasi-two-dimensional vortex pair issuing from the jet exhaust and also, Haven and Kurosaka (1997) illustrated the development of the primary steady and unsteady vortices (i.e., the kidney and anti-kidney vortices in their nomenclatures) with vortex filament methods. Likewise, development and interactions of the two CVP structures in the present parallel TJICF can be elucidated from cross-stream vorticity maps and the vortex filament sketch in Fig. 11. The small separation distance between the parallel TJICF spatially confines the growth of the pair of inner vortices (i.e., L2 and R2) and as a result, their vortex lines are compressed with reduced circulation as compared to the pair of outer vortices (i.e., L1 and R1). According to Biot-Savart's law, the induced velocity is directly proportional to the circulation strength of a vortex

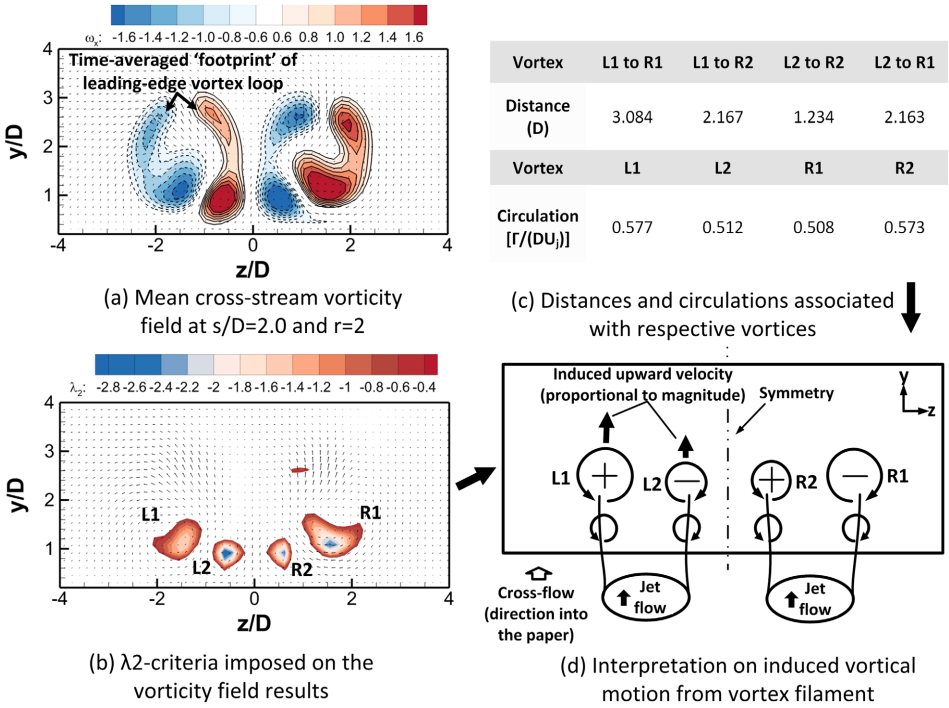

Vortex	L1 to R1	L1 to R2	L2 to R2	L2 to R1
Distance (D)	3.084	2.167	1.234	2.163
Vortex	**L1**	**L2**	**R1**	**R2**
Circulation [Γ/(DU$_j$)]	0.577	0.512	0.508	0.573

FIG. 11. A typical snapshot of the interactions between two CVPs of the parallel TJICF at s/D = 2 and r = 2, with a simplified vortex filament model in (d).

and inversely proportional to the distance between two vortices (i.e., $v_{induced} = \sum_{i=1}^{n} \frac{\Gamma_i}{2\pi d_i}$). Taking the CVP on the left for instance, the induced velocities associated with vortices L_1 and L_2, normalized by the jet exit mean velocity, are $(\frac{0.25}{\pi})$ and $(\frac{0.235}{\pi})$, respectively. Here, the circulation associated with each vortex and the distance between them have been estimated and summarized in Fig. 11(c) to allow a more precise estimate on the extents of the induced velocities. Moreover, peak λ_2 magnitude, $|\lambda_2|_{max}$, was selected to represent the centre of a vortex such that the distance between two vortices can be measured and the circulation can be obtained from surface integral of the vorticity with a 10% criterion (i.e., integrated over vorticity $|\omega_x| \geq 0.1|\omega_x|_{max}$). Note that a similar criterion has been implemented satisfactorily by Couch and Krueger (2011) in calculating the circulation associated with vortex-ring circulation.

Other than the different induced velocities, spatial confinement also contributes significantly towards the movements of the inner vortices, where both reinforce each other. As the inner vortices move closer towards each other due to spatial constraints, they begin to experience less upwards induced velocities and trail below the outer vortices. The trailing of the inner vortices below the outer vortices along the vertical direction as indicated in Fig. 11(d) can be clearly seen in Figs. 9(b) and 10(c) along x/D = 2 plane. This subsequently brings the two inner vortex cores even closer to each other until they undergo vorticity annihilation process. The annihilation of the opposite-signed inner vortices ensues and intensifies quickly when the pair of inner vortices approaches each other within a short downstream distance. As a result, the near-field merging of the CVPs arises from the continual vortical interactions and relative movements of the closely spaced parallel TJICF, as can be characterized and explained from the simplified vortex filament model.

D. Near-field circulation decay

Changes in the jet circulation provide direct and quantitative clues on the near-field developments of the large-scale coherent structures and the jet entrainment capabilities for the SJICF and parallel TJICF studied here. Hence, streamwise circulation decays for both SJICF and parallel TJICF are obtained by determining the circulations associated with each progressively downstream cross-stream plane and shown in Fig. 12. To determine the integration areas for circulation evaluations, a cut-off criterion of $|\omega_x| \geq 0.1|\omega_x|_{max}$ was first imposed on the vorticity results, after which the circulation strengths can be calculated for the bounded regions. Convergence tests (not included here for the sake of brevity) confirmed that the cut-off criterion proved to be satisfactory in evaluating the total circulation strength relatively well, without introducing much background vorticity into the bounded integration area, which may yield erroneously larger circulation strengths. Comparing between the results for SJICF at r = 4 (i.e., blue triangles) and those calculated from the analytical model proposed by Karagozian (1986) and experimental measurements by Fearn and Weston (1974), a cut-off criterion of $|\omega_x| \geq 0.1|\omega_x|_{max}$ appears to yield reasonable circulation magnitudes and trends in its decay. This further attests to the validity of using similar criterion to determine the circulation associated with the CVPs earlier. At r = 4, Karagozian (1986) identified a peak circulation at approximately x/D = 1.6, after which the circulation gradually decreases into a power law trend. Karagozian (1986) argued from the notion that the CVP forms quickly in the near-field of a SJICF, though very limited experimental data on the near-field circulations are available for comparisons then. However, the present circulation results at both r = 2 and 4 see a minor rise in their magnitudes at approximately x/D = 1.5 and 2, respectively, which agree well with the analysis made by Karagozian (1986). Furthermore, this agreement also

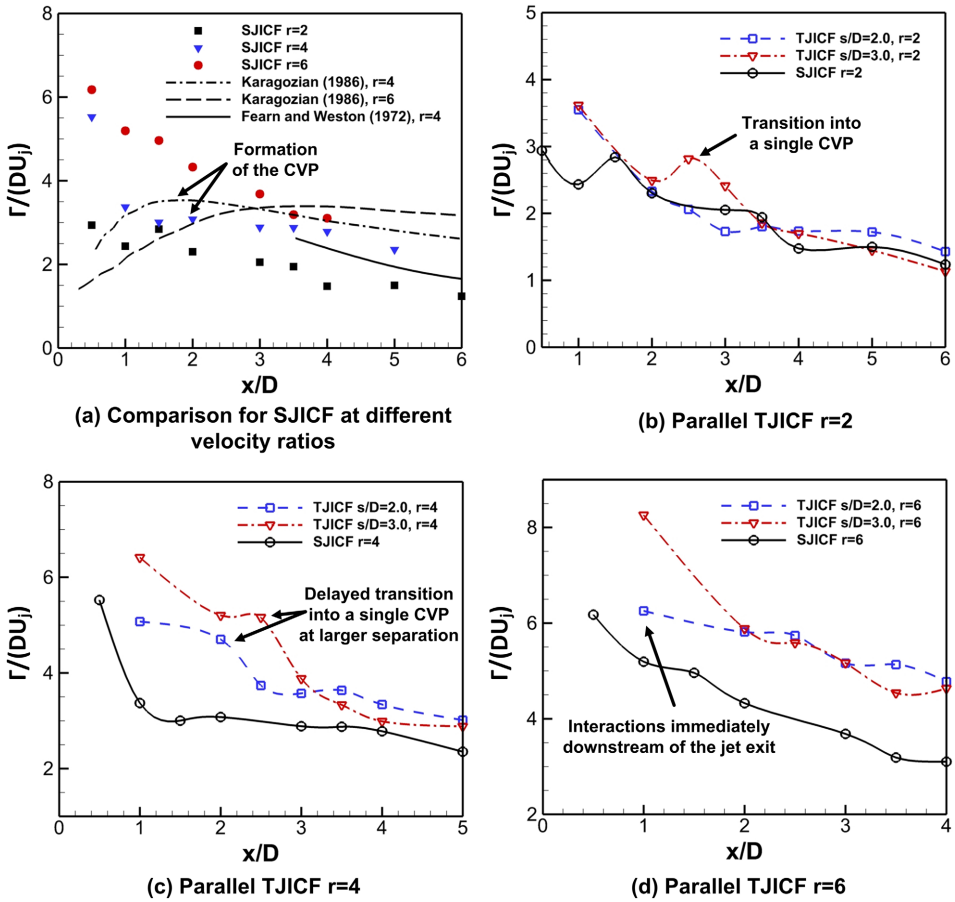

FIG. 12. Streamwise circulation decays determined from cross-stream vorticity fields with a cut-off criterion of 10% for (a) SJICF, and (b) r = 2, (c) r = 4, and (d) r = 6 of the parallel TJICF with s/D = 2.0 and 3.0 separation distances, respectively.

confirms that the CVP formation process takes place quickly and almost completes in the near-field for the present SJICF.

On the other hand, Figs. 12(b)–12(d) show the streamwise circulation decay trends for the s/D = 2.0 and 3.0 parallel TJICF at three different velocity ratios. Starting with approximately twice the strength at x/D = 1, circulations for both parallel TJICF decay rapidly to levels comparable to that of a SJICF further downstream, except at higher velocity ratios where the CVPs form and interact over a longer distance. Hence, circulations of parallel TJICF at r = 6 remain notably higher than their SJICF counterpart within the measurement window. More importantly, small fluctuations in the circulation can be observed for the parallel TJICF at r = 2 and 4 [see Figs. 12(b) and 12(c)], especially when the separation distance is larger. Although it resembles the peak associated with the formation of CVP in a SJICF, a closer examination on the corresponding vorticity fields in Figs. 9 and 10 reveals that these fluctuations in the circulations may be attributed to the fact that the cross-stream 2D PIV measurement planes are not perpendicular to the vortex lines that represent the CVPs in the resulting flow. Within the present measurement window, the vortex lines are continuously being deflected by the actions of the cross-flow and they are always inclined at some angles relative to the vertical cross-stream 2D PIV measurement planes. For the most accurate calculations of the circulation, the out-of-plane vorticity should be perpendicular to the measurement plane. Since that is not the case here, particularly closer to the jet exit (i.e., at smaller x/D locations), evaluation of circulation via cross-stream 2D PIV measurements may incur fluctuations due to the preceding scenario. Furthermore, it should be mentioned that there exist significant interactions between the various CVPs, which could have further contributed to the fluctuations. However, the increments only persist over a short downstream distance, before the opposite-signed vorticities begin to annihilate each other through mutual interactions. As the inner vortices continue to reduce in strength and a single CVP is eventually formed, circulations of the parallel TJICF become essentially similar to that of the SJICF. Therefore from the perspective of jet circulation, an increase in the entrainment level is only expected to be close to the jet exits for a closely spaced parallel TJICF where the CVP structures are still interacting.

E. Mean Reynolds shear stresses

To provide further insights into the development of parallel TJICF CVP structures and their associated entrainment characteristics, Reynolds shear stresses along different cross-stream planes were determined and Fig. 13 shows their results for both SJICF and parallel TJICF at a relatively low velocity ratio of r = 2 with x/D = 1 intervals in the downstream direction. The shear stresses are non-dimensionalized by the square of the mean cross-flow velocity (i.e., $\overline{v'w'}/U_\infty^2$) in order to allow more direct comparisons. As can be observed for the reference SJICF results in Fig. 13(a), regions of high flow shear stresses initially concentrate around the shear layers between the jet column and the cross-flow as the jet continues to penetrate into the cross-flow prior to incurring significant deflections. This is within expectation as significant amount of cross-flow fluid

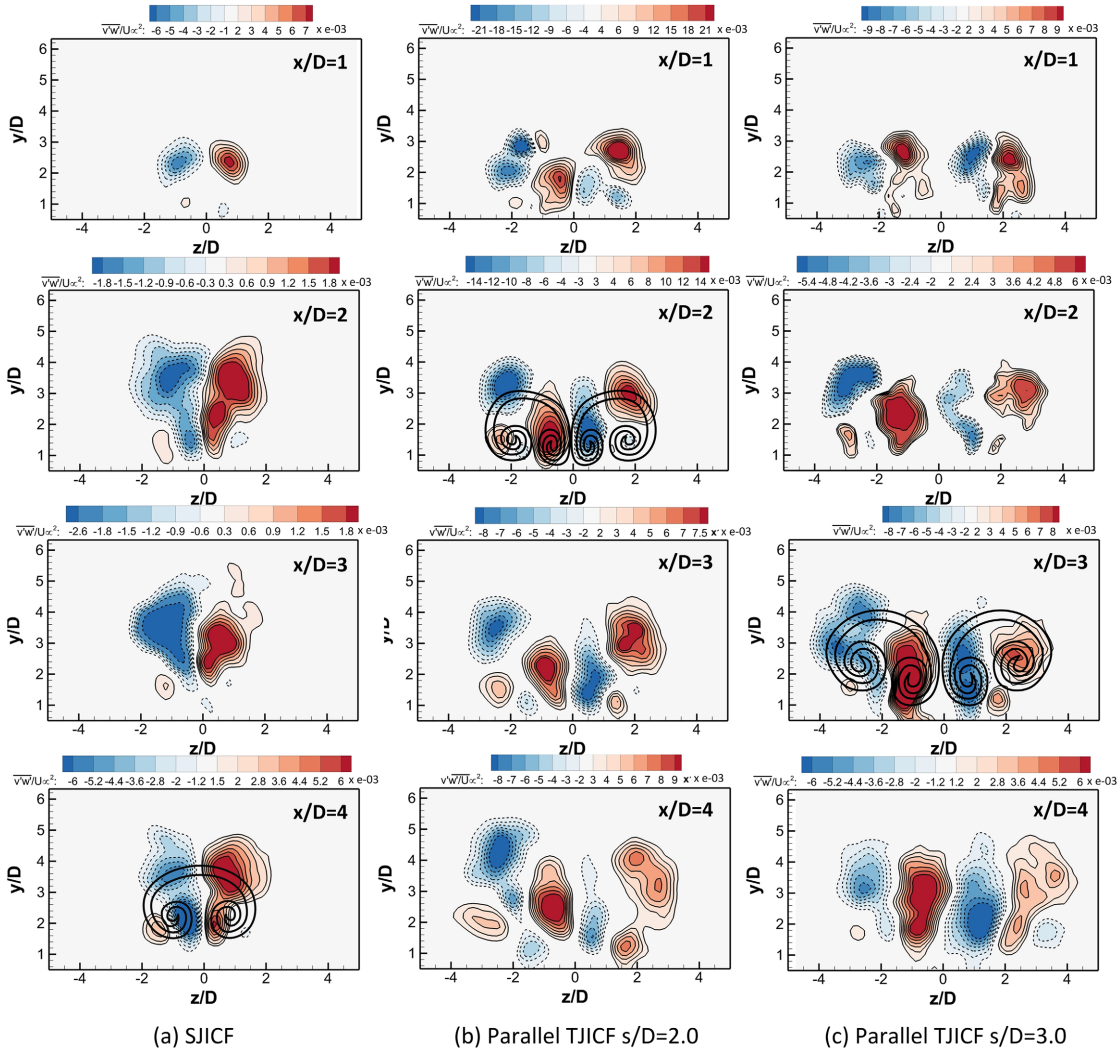

FIG. 13. Mean Reynolds shear stress ($\overline{v'w'}/U_\infty^2$) distributions along different cross-stream measurement planes for (a) SJICF, (b) s/D = 2, and (c) s/D = 3 parallel TJICF at a relatively lower velocity ratio of r = 2.

is entrained by the shear layer vortices (i.e., leading-edge and lee-side vortices) within the near-field. Moving further downstream, growth in the flow shear stresses close to the symmetry below the jet column can be further observed, where the CVP structure develops into the dominant coherent structure responsible for cross-flow fluid entrainment (see the corresponding sketch in Fig. 13(a) at x/D = 4 location).

For the s/D = 2 parallel TJICF, the pair of inner vortices begins to interact almost immediately downstream of the jet exit, and hence, notable levels of flow shear stresses can be observed both between each individual jet column and the cross-flow, as well as within the CVPs, as can be seen in Fig. 13(b) at x/D = 2 location. The flow shear levels between the latter are expected to reduce as they undergo vorticity annihilation, with the parallel TJICF beginning to resemble closer to that of the reference SJICF scenario in terms of the mean Reynolds shear stress distribution. Note that, however, the former is more spatially dispersed, due to larger distance between the two outer vortices. Moreover, since flow shear stresses in this case are related to the entrainment of the cross-flow fluid, it can be inferred that constant shearing between the pair of inner vortices is likely to enhance cross-flow fluid entrainment in regions adjacent to the symmetry plane of the parallel TJICF. Next, recall from the cross-stream vorticity results in Fig. 9 that interactions between the two CVPs are delayed to further downstream location in parallel TJICF at r = 2 when the separation distance increases to s/D = 3. Similar results can also be observed from the mean Reynolds shear stress of the s/D = 3 parallel TJICF, shown in Fig. 13(c). Unlike the s/D = 2 configuration, the two jets can be seen to behave almost independently at x/D = 1 location, even though they do subsequently develop into structures similar to that of the s/D = 2 parallel TJICF at x/D = 3 location. Note that sketches of the CVP structures are included in Fig. 13(b) at x/D = 2 and Fig. 13(c) at x/D = 3, respectively, for better comparisons between the two different separation distances.

It is also interesting to note from Figs. 13(a)–13(c) that the mean flow shear stress magnitudes for SJICF are generally lower than those for parallel TJICF, particularly at x/D = 1 location. As mentioned earlier, the initial turbulence intensity levels increase when a second jet is placed at close proximity to the first one. Hence, the initially higher turbulence intensity levels in parallel TJICF are expected to lead to higher flow shear stress levels, which are further increased when the pair

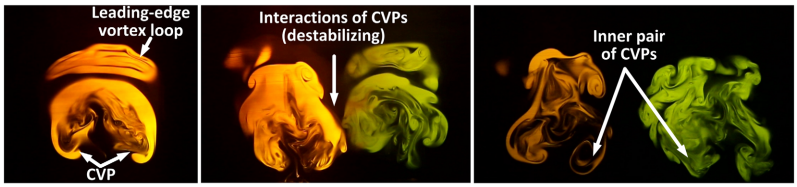

FIG. 14. Instantaneous LIF snapshots for (a) SJICF, (b) s/D = 2.0, and (c) s/D = 3.0 parallel TJICF along x/D = 1D location at a relatively lower velocity ratio of r = 2.

of inner vortices begins to interact and destabilize each other. Visual inspections of the instantaneous LIF visualization images for both SJICF and parallel TJICF at x/D = 1 location in Fig. 14 support the notion arising from the flow shear stress results that the CVP structure and jet column are more coherent in the SJICF than the parallel TJICF. Figure 15 shows the mean Reynolds shear stress results of the SJICF and parallel TJICF when the velocity ratio increases to r = 6. Since formation of

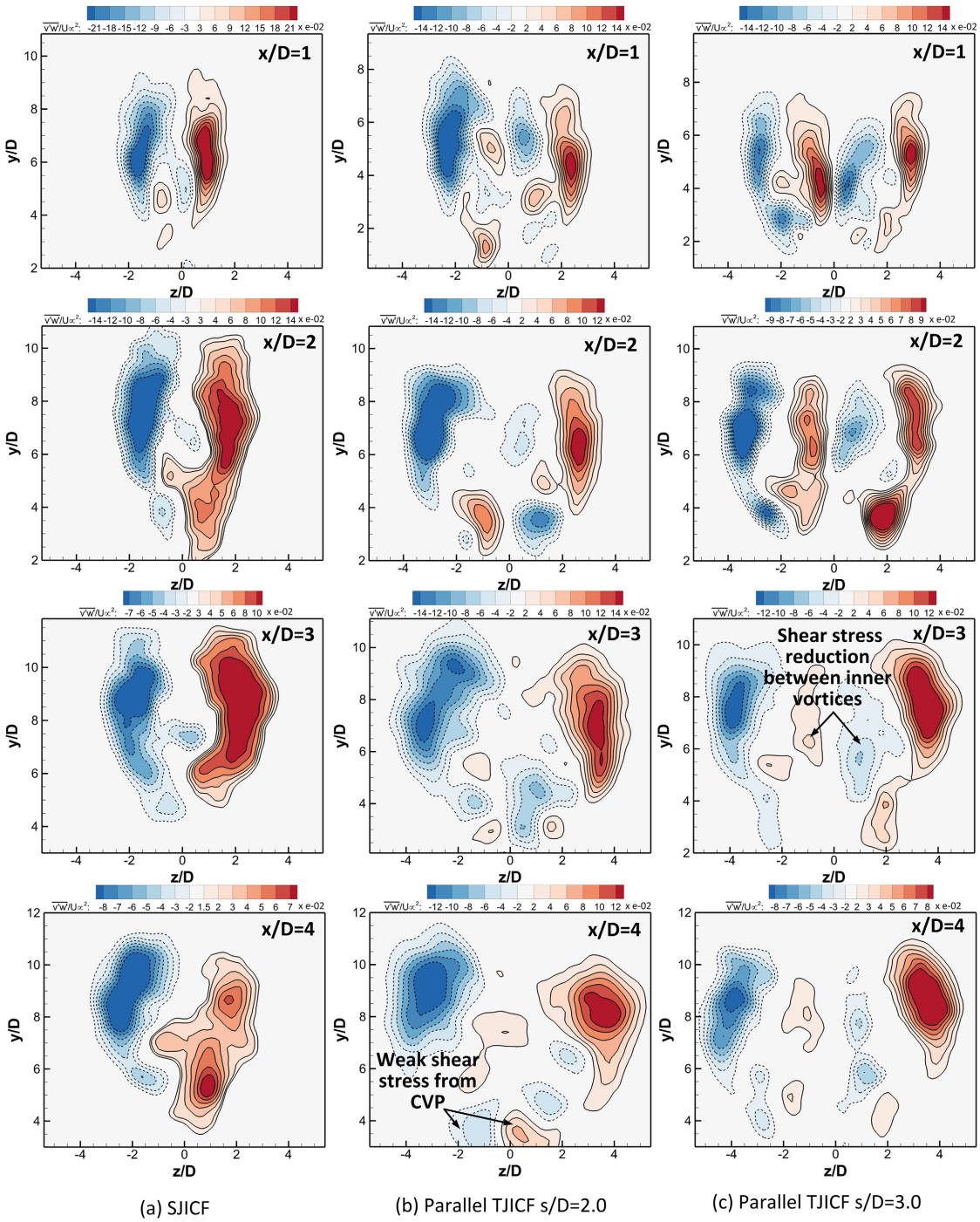

FIG. 15. Mean Reynolds shear stress $(\overline{v'w'}/U_\infty^2)$ distributions along the cross-stream measurement planes for (a) SJICF, (b) s/D = 2, and (c) s/D = 3 parallel TJICF at a higher velocity ratio of r = 6.

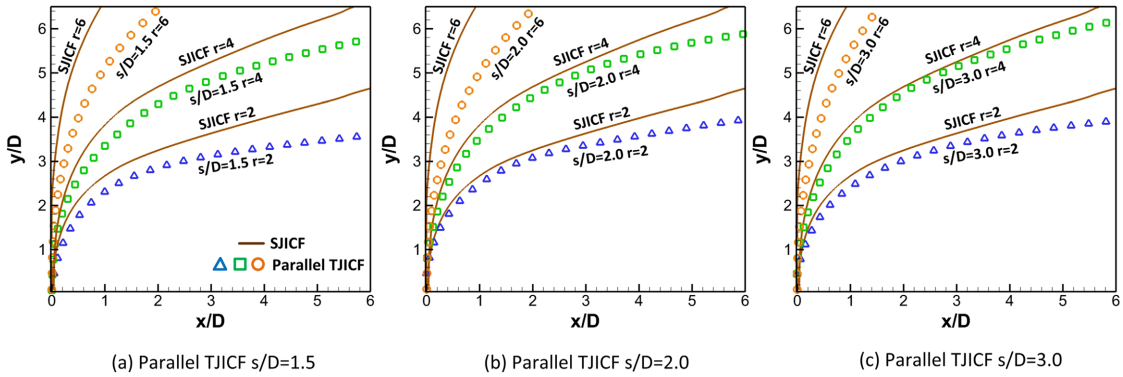

FIG. 16. Comparisons of mean jet trajectories determined from DPIV measurements for parallel TJICF at (a) s/D = 1.5, (b) s/D = 2.0, and (c) s/D = 3.0 with SJICF at similar velocity ratios as references.

shear layer vortices intensifies in the near-field while formation of the CVP structure is yet to complete at higher velocity ratio, the shear stress distributions can be observed to concentrate primarily along the shear layers between the jet column and the cross-flow for both SJICF and parallel TJICF. However, relatively weak flow shear stresses associated with the CVP structures can be seen in Figs. 15(a)–15(c) at x/D = 4 location. More importantly, the flow shear stress distributions confirm that even at a higher velocity ratio, annihilation of the inner vortices takes place quickly over a short downstream distance, which manifests as the flow shear stress undergoes rapid reduction along the symmetry plane as shown in Fig. 15(c).

F. Near-field jet trajectories

Lastly, the near-field jet trajectories of the SJICF and parallel TJICF (i.e., the trajectories of one jet in the twin jet configurations) were extracted from the mean streamlines originating at the jet exit centre in a similar manner as determining the jet half-width, and shown in Fig. 16. Clearly, the jets in a parallel TJICF penetrate less into the cross-flow than if they were configured as SJICF for all separation distances and velocity ratios. This is not surprising, as the close proximity of the inner pair of vortices mutually induces a small downward-acting velocity on the adjacent jet columns as depicted in Fig. 11(d), which becomes stronger when the separation distance decreases. Furthermore, having a larger jet half-width in the near-field, parallel TJICF entrains more cross-flow fluid in the streamwise direction than their SJICF counterpart, which leads to greater deflections at corresponding velocity ratios. Extending this argument further, the parallel TJICF with the smallest separation distance (i.e., s/D = 1.5) can be expected to penetrate the least into the cross-flow, which can be observed in Figs. 16(c)–16(a). Hence, the near-field trajectory results not only corroborate the observations made by Holdeman *et al.* (1997) previously but also indicate higher near-field entrainment capabilities of a parallel TJICF configuration as the separation distance decreases, at least under the present experimental conditions.

IV. CONCLUSIONS

LIF and DPIV experiments were conducted on parallel TJICF with three jet-to-jet separation distances (i.e., s/D = 1.5, 2, and 3) and three velocity ratios (i.e., r = 2, 4, and 6). Flow visualization results show that the leading-edge and lee-side vortices form closer to the jet exits for parallel TJICF than those for a SJICF, consistent with the expected increase in mutual interactions between closely spaced parallel jets. As deduced from the vertical velocity component profiles along the jet plane, near-field developments of parallel TJICF bear resemblance to a SJICF if their velocity ratio or separation distance increases. Conversely, when measured along the parallel TJICF symmetry plane, corresponding velocity profiles exhibit characteristics comparable to a SJICF when the parallel TJICF separation distance is decreased. In fact, instantaneous vorticity results along the symmetry plane of the s/D = 1.5 parallel TJICF reveal the presence of organized large-scale coherent structures similar to the leading-edge and lee-side vortices. Subsequently, jet half-widths determined along the jet mean trajectories confirm that each jet in the parallel TJICF configuration generally has larger jet spreads than a SJICF. Moreover, parallel TJICF jet half-widths experience rapid increases beyond the potential core region, where significant jet deflections occur. The results support the analysis by Yuan *et al.* (1999) on the streamwise entrainment of the cross-flow fluid by the deflected jet.

Cross-stream measurements reveal that two CVPs, one from each jet in the parallel TJICF configuration, are observed to undergo significant interactions in the near-field, during which the pair of inner vortices undergoes mutual annihilation. It has been demonstrated also that a simplified vortex filament model, coupled with spatial confinement, is able to account for the induced motions of the inner and outer vortices that lead to increasingly intensified annihilation of the inner opposite-signed vorticities. Under the present experimental conditions, this process takes place rapidly within the near-field region with the exception of the s/D = 3 parallel TJICF at a velocity ratio of r = 2. Although the exact topological developments depend on the exact separation distance and velocity ratio, a single resulting CVP from the parallel TJICF configurations can be expected to exist in the far-field as a result of the preceding vorticity annihilation process. Furthermore, jet circulations are determined from DPIV measurements and analysis of their decays corroborates with the notion that a single merged CVP structure will arise from the two CVPs produced by parallel TJICF. Interestingly, CVP circulations determined along the cross-stream measurement planes increase momentarily when the CVPs begin to interact. This is possibly due to the CVP

vortex lines not aligned perpendicularly to the cross-stream measurement planes, as well as the fact that the CVPs are constantly compressed within the confined space. Lastly, mean Reynolds shear stress results illustrate the gradual decrease and increase of the flow shear stresses associated with the jet shear layers and CVP structures of parallel TJICF, respectively, as the jets exhaust from their exits and convect downstream. More importantly, a region of high flow shear stresses can also be observed when the pair of inner vortices interacts, which is likely to contribute to the heightened levels of cross-flow fluid entrainment close to the symmetry plane. Both the wider jet half-width and greater Reynolds shear stresses observed in parallel TJICF corroborate with the jet trajectory results in which the trajectory of each jet in the relatively closely spaced parallel TJICF here is always lower than that of SJICF at similar velocity ratios.

ACKNOWLEDGMENTS

The authors acknowledge the support for the study by a Nanyang Technological University Start-Up Grant and Singapore Ministry of Education AcRF Tier-2 grant (Grant No. MOE2014-T2-1-002). The first author is also grateful for the financial support provided by a Nanyang Technological University Ph.D. Research Scholarship.

Ajersch, P., Zhou, J. M., Ketler, S., Salcudean, M., and Gartshore, I. S., "Multiple jets in a crossflow: Detailed measurements and numerical simulations," J. Turbomach. **119**, 330–342 (1997).

Andreopoulos, J. and Rodi, W., "Experimental investigation of jets in cross flow," J. Fluid Mech. **138**, 93–127 (1984).

Becker H. A. and Massaro T. A., "Vortex evolution in a round jet," J. Fluid Mech. **31**, 435–448 (1968).

Broadwell, J. E. and Breidenthal, R. E., "Structure and mixing of a transverse jet in incompressible flow," J. Fluid Mech. **148**, 405–412 (1984).

Cambonie, T., Gautier, N., and Aider, J. L., "Experimental study of counter-rotating vortex pair trajectories induced by a round jet in cross-flow at low velocity ratios," Exp. Fluids **54**, 1475 (2013).

Cortelezzi, L. and Karagozian, A. R., "On the formation of the counter-rotating vortex pair in transverse jets," J. Fluid Mech. **446**, 347–373 (2001).

Couch, L. D. and Krueger, P. S., "Experimental investigation of vortex rings impinging on inclined surfaces," Exp. Fluids **51**, 1123–1138 (2011).

Fearn, R. and Weston, R. P., "Vorticity associated with a jet in a cross flow," AIAA J. **12**, 1666–1671 (1974).

Findlay, M. J., Salcudean, M., and Gartshore, I., "Jets in a crossflow: Effects of geometry and blowing ratio," Trans. ASME – J. Fluids Eng. **121**, 373–378 (1999).

Fric, T. F., "Structure in the near field of the transverse jet," Ph.D. thesis, California Institute of Technology, 1990.

Fric, T. F. and Roshko, A., "Vortical structure in the wake of a transverse jet," J. Fluid Mech. **279**, 1–47 (1994).

Gogineni, S., Goss, L., and Roquemore, M., "Manipulation of a jet in a cross flow," Exp. Therm. Fluid Sci. **16**, 209–219 (1998).

Haven, B. A. and Kurosaka, M., "Kidney and anti-kidney vortices in crossflow jets," J. Fluid Mech. **352**, 27–64 (1997).

Holdeman, J. D., Liscinsky, D. S., and Bain, D. B., "Mixing of multiple jets with a confined subsonic crossflow: Part II—Opposed rows of orifices in rectangular ducts," ASME Trans. - J. Eng. Gas Turbines Power **121**, 551–562 (1999).

Holdeman, J. D., Liscinsky, D. S., Oechsle, V. L., Samuelsen, G. S., and Smith, C. E., "Mixing of multiple jets with a confined subsonic crossflow: Part I—Cylindrical duct," ASME Trans. - J. Eng. Gas Turbines Power **119**, 852–862 (1997).

Holdeman, J. D. and Walker, R. E., "Mixing of a row of jets with a confined crossflow," AIAA J. **15**, 243–249 (1977).

Jeong, J. H. and Hussain, F., "On the identification of a vortex," J. Fluid Mech. **285**, 69–94 (1995).

Karagozian, A. R., "An analytical model for the vorticity associated with a transverse jet," AIAA J. **24**, 429–436 (1986).

Karazogian, A. R., "The jet in crossflow," Phys. Fluids **26**, 101303 (2014).

Keane, R. D. and Adrian, R. J., "Theory of cross-correlation analysis of PIV images," Appl. Sci. Res. **49**, 191–215 (1992).

Kelso, R. M., Lim, T. T., and Perry, A. E., "An experimental study of round jets in cross-flow," J. Fluid Mech. **306**, 111–144 (1996).

Kolář, V. and Savory, E., "Dominant flow features of twin jets and plumes in crossflow," J. Wind Eng. Ind. Aerodyn. **95**, 1199–1215 (2007).

Kolář, V., Takao, H., Todoroki, T., Savory, E., Okamoto, S., and Toy, N., "Vorticity transport within twin jets in crossflow," Exp. Therm. Fluid Sci. **27**, 563–571 (2003).

Lim, T. T., New, T. H., and Luo, S. C., "On the development of large-scale structures of a jet normal to a cross flow," Phys. Fluids **13**, 770–775 (2001).

Lim, T. T., New, T. H., and Luo, S. C., "Scaling of trajectories of elliptic jets in cross-flow," AIAA J. **44**, 3157–3160 (2006).

Long, J. and New, T. H., "A DPIV study on the effects of separation distance upon the vortical behaviour of jet-cylinder impingements," Exp. Fluids **56**, 153 (2015).

Margason, R. J., "Fifty years of jet in crossflow research," in *AGARD Symposium on a Jet in Crossflow*, AGARD-CP-534 (NATO, Winchester, UK, 1993).

Mahesh, K., "The interactions of jets with crossflow," Annu. Rev. Fluid Mech. **45**, 379–407 (2013).

Marzouk, Y. M. and Ghoniem, A. F., "Vorticity structure and evolution in a transverse jet," J. Fluid Mech. **575**, 267–305 (2007).

Moffat, R. J., "Describing the uncertainties in experimental results," Exp. Therm. Fluid Sci. **1**, 3–17 (1988).

Muppidi, S. and Mahesh, K., "Study of trajectories of jets in crossflow using direct numerical simulations," J. Fluid Mech. **530**, 81–100 (2005).

Muppidi, S. and Mahesh, K., "Two-dimensional model problem to explain counter-rotating vortex pair formation in a transverse jet," Phys. Fluids **18**, 085103 (2006).

New, T. H., "Near-field developments of elliptic jets in crossflow," J. Turbul. **9**, N24 (2008).

New, T. H., Lim, T. T., and Luo, S. C., "Elliptic jets in cross-flow," J. Fluid Mech. **494**, 119–140 (2003).

New, T. H., Lim, T. T., and Luo, S. C., "A flow field study of an elliptic jet in cross flow using DPIV technique," Exp. Fluids **36**, 604–618 (2004).

New, T. H., Lim, T. T., and Luo, S. C., "Effects of jet velocity profiles on a round jet in cross-flow," Exp. Fluids **40**, 859–875 (2006).

New, T. H. and Zang, B., "On the trajectory scaling of tandem twin jets in cross-flow in close proximity," Exp. Fluids **56**, 1–12 (2015).

Nun, R. H., "Vorticity growth and decay in jet in cross flow," AIAA J. **23**, 473–475 (1985).

Pratte, B. D. and Baines, W. D. "Profiles of the round turbulent jet in a cross-flow," J. Hydraul. Div., Am. Soc. Civ. Eng. **92**, 53–64 (1967).

Raffel, M., Willert, C. E., Wereley, S. T., and Kompenhans, J., *Particle Image Velocimetry—A Practical Guide*, 2nd ed. (Springer, New York, 2007).

Savory, E. and Toy, N., "Real-time video analysis of twin jets in a crossflow," ASME Trans.—J. Fluid Eng. **113**, 68–72 (1991).

Schlichting, H. and Gersten, K., *Boundary Layer Theory*, 8th ed. (Springer, New York, 2000).

Schlüter, J. U. and Schönfeld, T., "LES of jets in cross flow and its application to gas turbine burner," Flow, Turbul. Combust. **65**, 177–203 (2000).

Sherif, S. A. and Pletcher, R. H., "Measurements of the flow and turbulence characteristics of round jets in crossflow," ASME Trans.—J. Fluid Eng. **111**, 165–171 (1989).

Smith, S. H. and Mungal, M. G., "Mixing, structure and scaling of the jet in crossflow," J. Fluid Mech. **357**, 83–122 (1998).

Toy, N., Savory, E., McCusker, S., and Disimile, P. J., "The interaction region associated with twin jets and a normal crossflow," in *AGARD Symposium on a Jet in Crossflow*, AGARD-CP-534 (NATO, Winchester, UK, 1993).

Westerweel, J., "Fundamentals of digital particle image velocimetry," Meas. Sci. Technol. **8**, 1379–1392 (1997).

Yuan, L. L. and Street, R. L., "Trajectory and entrainment of a round jet in crossflow," Phys. Fluids **10**, 2323-2335 (1998).

Yuan, L. L., Street, R. L., and Ferziger, J. H., "Large-eddy simulations of a round jet in crossflow," J. Fluid Mech. **379**, 71–104 (1999).

Zaman, K. B. M. Q. and Foss, J. K., "The effect of vortex generators on a jet in a cross-flow," Phys. Fluids **9**, 106–114 (1997).

Zang, B. and New, T. H., "On the wake-like vortical arrangement and behaviour associated with twin jets in close proximity," Exp. Therm. Fluid Sci. **69**, 127–140 (2015).